Appendix F—Distribution of Slip in Ruptures

By Glenn P. Biasi,[1] Ray J. Weldon, II,[2] Timothy E. Dawson[3]

Introduction

We investigate the distribution of slip to be applied to ruptures in the Grand Inversion (GI) of the Uniform California Earthquake Rupture Forecast, version 3, (UCERF3). The GI (appendix N, this report, 2013; Field and Page, 2011) will be used to invert for the frequency of rupture for every fault in the California model. Inputs to the GI include fault slip rates, background seismicity rates, slip-rate reductions due to creep, regional magnitude-frequency relationships, and paleoseismic rupture investigations. To compare fault slip rates to slip rates inferred from ground rupture frequencies, an average displacement function is required. The displacement function used in the GI is not the displacement of any specific ground rupture but rather the average displacement expected if one had many repeats of each earthquake and could average the displacement across all the repeats. Although individual surface rupture displacement profiles are generally extremely variable, the average over many repeats of that earthquake will be much smoother. The goal of this appendix is to describe how the average displacement shape is developed for the specific needs of the GI.

An issue in using empirical ground-rupture data is that the number of well-mapped surface ruptures is relatively small. In addition slip in ground ruptures varies significantly from one rupture to the next. As a result, the approach taken here is to seek an average rupture shape across all available ruptures, while checking for any systematic differences among subsets, say between ruptures with small aspect ratios versus large ones.

Within the Grand Inversion faults are divided into subsections whose length along strike is constrained to be half of the seismogenic thickness at that point. Thus, subsections are typically about 7.5 kilometers (km) long and 15 km in depth and vary somewhat around these dimensions depending on location. Discrete earthquakes can occur in the GI on any two or more adjacent subsections, and can include fault-to-fault jumps up to some maximum allowed separation distance. Separate ruptures developed for input to the inversion thus consist of adjacent 2, 3, 4, … subsections, lengthening until the end(s) of the fault are encountered. The Inversion seeks to invert for the frequency of each rupture. For each rupture the distribution of slip on rupture r, D_r, is divided among subsections s, with the slip on individual subsections denoted D_{sr}. The frequency with which ruptures occur is roughly the slip rate divided by the average value for D_{sr}.

An issue for the distribution of slip applied in the GI to individual ruptures is how to apply slip to ruptures that jump from one fault to another. The slip must end on the first fault and

[1] University of Nevada, Reno.
[2] University of Oregon.
[3] California Geological Survey.

increase from zero on the second. Thus, the net displacement profile could have a dip in the middle at the fault-to-fault jumping point, or the two may overlap in such a way that the total between the two is relatively continuous. An additional issue is whether the average displacement is similar between a simple fault rupture and one of the same combined length with fault-to-fault jumps in it and whether the displacements scale with the total rupture length or with the lengths of the contributing fault pieces. We find from empirical ruptures that the total length in fault-to-fault rupture cases is the more relevant scale for setting rupture displacement D_r.

Model Rupture Shapes

Candidate shapes for slip distribution include uniform ("boxcar"), triangular, and empirical. Wesnousky (2008) fit triangular shapes to observed ruptures but found that they did not predict much of the data. Even for the limited extent that the triangular shape can be made to fit, they require knowledge of the rupture direction to apply prospectively. It would not be a preferred shape as an input to the GI because GI input rupture profiles are expected averages over many occurrences of the same event. Biasi and Weldon (2006) found that after ruptures are normalized by length and average displacement, their averaged functional form is well approximated by:

$$D(x)=1.311\times[\sin(\pi x)]^{1/2} \quad (1)$$

for $x: \{0 \le x \le 1\}$. Displacement $D(l)$ for ruptures scaled by this function would then have the value

$$D(l)=1.311\ AD\ [\sin(\pi l/L)]^{1/2} \quad (2)$$

where AD is the average surface rupture displacement, L is the rupture length, and l is in the range $\{0 \le l \le L\}$. The constant prefactor 1.311 is one divided by the average of the $[(\sin(\pi x)]^{1/2}$ term. Equation 1 has sometimes been called the *sinesqrt* function. This shape works well for the average if all ruptures are considered, as well as for subsets such as ruptures shorter than 30 km and ruptures longer than 200 km. In addition, the *sinesqrt* function can be used without knowing the rupture direction. The fact that a single shape fits subsets of short and long strike-slip ruptures suggests some sort of self-similarity in the gross mechanics of ground rupture. A general arcuate shape of the net rupture profile across fault-to-fault interactions also emerged from boundary element and finite-difference models (Willemse and others, 1996; Kase, 2010). Willemse and others (1996) and Kase (2010) found general support for a slip distribution that is somewhat flattened in the middle, with the specific shape depending on how the model is structured and how many elements are interacting. In general, these models require more information than is presently available for UCERF3 ruptures. Also, the set of normalized empirical ruptures seems to include similar degrees of variation without introducing complications about how it arises. As such, it is the focus of the proposed implementation of D_{sr}.

The distribution of slip in surface ruptures can be approached empirically or theoretically. The empirical approach seeks ways to generalize and apply observations of previous ground ruptures. The theoretical approach draws from studies of strain and displacement in elastic media. In general, the two approaches agree quite well, suggesting that the essential properties of rupture displacement are being represented.

Empirical Rupture Shape

A basic problem for using observed ruptures is that the database of well-mapped ruptures is small and ruptures vary significantly from one to another. This means that for any given rupture length there are too few past ruptures of similar size to develop a statistically meaningful representation. Hemphill-Haley and Weldon (1999) addressed this problem by converting ruptures to unit lengths and normalizing by average displacement. After converting ruptures to unit length, they can be compared to one another and investigated for systematic properties. This approach does make the assumption that the degree of slip variability among small and large ruptures is similar, but based on the limited available data, this assumption seems satisfactory (Shaw, 2011; Biasi and Weldon, 2006). Stacking the normalized ruptures and using their averaged shape yields the empirical shape for rupture profiles.

To develop an averaged rupture shape we used 22 strike-slip ruptures from Wesnousky (2008). Two approaches are considered in developing the average. The first approach includes each rupture only once, either as plotted in the original paper, or otherwise, such as with the epicenter on one side, to look for systematics in rupture propagation. Wesnousky (2008) explored these possibilities at some length, but did not find any compelling directionality effects or reasons to adopt, a priori, an asymmetric rupture shape. The second approach is to recognize that the plotting convention for ruptures is arbitrary and to include in the average each rupture and its left-to-right reflection. The arbitrariness of the plotting convention is seen in the fact that any asymmetry in the rupture would be left-to-right reversed by plotting it from the opposite side of the fault. By stacking ruptures and their reflections, the result is less subject to accidents of presentation. Averaging over many ruptures is done because fault-by-fault knowledge of characteristic rupture shapes is generally not available. If somehow a characteristic rupture is known to occur on a particular fault, use of the averaged rupture profile shape would not be appropriate.

Figure F1 provides results of the averaging process for the complete set and selected subsets of Wesnousky (2008) strike-slip ruptures. In each figure the average is shown for unreflected and reflected rupture stacks. Short ruptures are seen to have similar average shapes compared to longer subsets. The averaged shape for the longest ruptures is of interest to see whether the rupture shape flattens in the middle, perhaps because slip could saturate when the rupture is many times longer than the depth W of the seismogenic crust. There is some suggestion to this effect among the L>200 km ruptures, but not so strong a case as to recommend an additional parameter. The L<30 km set examines whether low aspect ratio ($L<\sim 2W$) ruptures differ, perhaps because more rupture is below the surface. The L<75 km set ($L<5W$) and L>75 km set explore the middle ground where L is a few times the depth of the seismogenic layer. The model shape of equation 1 is drawn on each set of profiles. The *sinesqrt* shape captures the averaged shape remarkably well considering that it is not fit to the data (or equally, plotted with no adjusted parameters). The ensemble of plots is intended to show that the model shape works well at all aspect ratios and that separate functional forms do not appear necessary. If a formal fit to the displacement data was desired, the observed data might be better respected by cutting each displacement profile at its mid-point, then fitting the total ensemble of half-widths to the model shape. That the same model shape would work well both for the shortest and longest subsets of ruptures suggests that some sort of self-similarity exists among the rupture sets. Figure F2 shows the one-standard deviation range of normalized displacements for the strike-slip ruptures greater than 200 km in length. The mean displacement and model shape are repeated from figure F1. As may be seen, the range of normalized displacements is large enough that it would be difficult to

prove the value of additional fitting parameters to modify equation 1 such as to accommodate saturation of displacement for ruptures much longer than the thickness of the seismogenic crust.

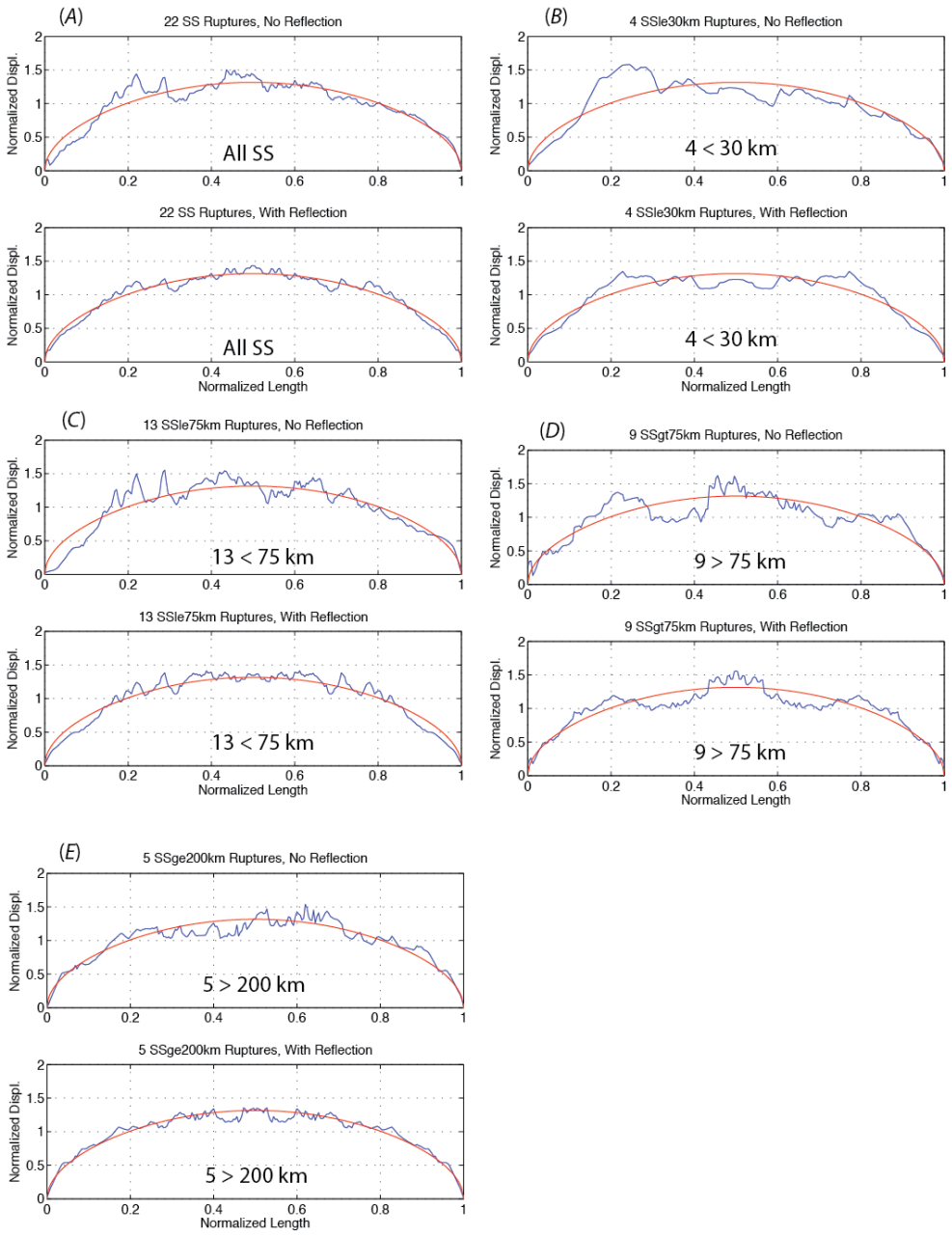

Figure F1. Strike-slip rupture profiles averaged in groups by length. *A*, The complete set with no length subsetting. The blue line is the average normalized displacement. For each pair of plots, the upper panel averages ruptures as they are plotted in their original reports; in the lower panel we include a reflection of each rupture in the average. The *sinesqrt* shape (equation 1) is in red. *B*, Four ruptures shorter than 30 kilometers (km). *C*, 13 profiles <75 km in length. *D*, Nine profiles >75 km, or at least five times a nominal seismogenic crustal thickness of 15 km. *E*, 5 profiles >200 km. The simple and reflected shapes are very similar. A tendency for saturation of slip suggested in the >75 km set is not observed in the longest ruptures.

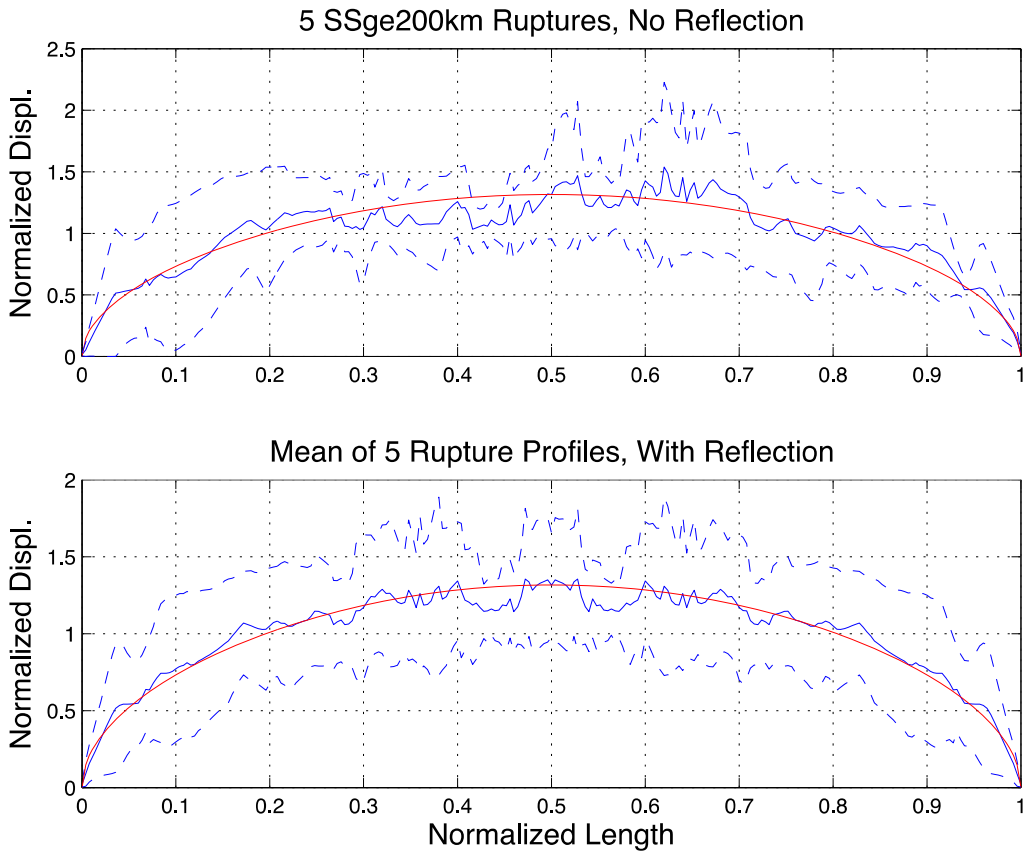

Figure F2. Plots showing one standard deviation of ranges of normalized displacements for five strike-slip ruptures longer than 200 kilometers (km). Upper, unreflected rupture profiles. Lower, original and reflected profiles. The mean (solid blue) and model (red line) are repeated from the corresponding plots in figure F1.

We looked briefly into why the *sinesqrt* shape might work as well as it does. Eschelby (1957) found that a uniform stress-drop patch in a homogeneous, isotropic, linear elastic space will be elliptical. The ellipse concentrates stress at the crack edge into an apparent singularity. Studies by Ingraffea (1987), Vermilye and Scholz, (1998), Cowie and Scholz (1992), Okubo and Dieterich (1984), and Martel and Pollard (1989), among others, have examined this problem. A process zone of nonlinear behavior, microfracture or off-fault failure of some sort is inferred at the crack tip. Wilkins and Schultz (2005) synthesized previous work into a model end of rupture they termed a “cohesive end zone” (CEZ). The CEZ is a zone near the crack tip in which resolved shear stress along the fault is matched by back shear stresses. The back stresses are modeled as a zone of increasing normal stress that acts with friction to resist and ultimately to counteract the shear stress and arrest rupture. In their model, displacement on the rupture is tapered and decreases asymptotically to the end, instead of having a maximum displacement gradient at the crack tip. This taper reduces the displacement gradient and the singularity. Without needing to endorse any specific model of processes at the ends, the CEZ model flattens the displacement profile relative to an ellipse. It is also likely that the shear stresses on the fault are not uniform but tapered, because faults have little or no intact material to fracture. It appears that relative to a model elliptical surface rupture, the more tapered *sinesqrt* shape better matches

real ruptures because it represents more of the of the physics of what is happening at the ends of ground ruptures.

Normalizing measured surface rupture profiles by average displacement removes the differences between rupture displacements caused by variations in stress drop. However, variations in stress drop contribute to the spread of real data around an *L-AD* regression (for example, Wells and Coppersmith, 1994). Therefore, variability in average displacement can be preserved in the GI by sampling from the uncertainty in the average displacement versus rupture length (*AD(L)*) relation. Details of UCERF3 regression relations and their uncertainties are in appendix E (this report).

Alternative Rupture Shapes

The GI also considers the uniform (boxcar) distribution as a logic-tree element. The differences between the boxcar and *sinesqrt* were discussed in a June 2011 workshop. The main conclusion from that discussion was that the rupture shape should be matched to the slip-rate gradients at fault ends and steps. Specifically, if a tapered rupture shape such as the *sinesqrt* is applied, then slip rates should taper toward fault ends and major step-overs. If ruptures are assigned a uniform shape, the slip rates should continue to the end of the fault so that net slip can be matched. If slip rates are not tapered, but the rupture profile is, there will be some tendency in the inversion to match the fault slip rate by adding extra small ruptures at the fault ends.

The Effect of Enveloping on Average Displacement

In Wesnousky (2008) the average displacements of ruptures were calculated from the point measurements of displacement reported in the original field studies. In some cases the displacements almost certainly underestimate the slip at, say, a kilometer depth (for example, the Parkfield earthquake, Langbein and others, 2006). This can occur when near-surface geologic layers absorb deformation as distributed subsurface fracturing or particle rotations. The potential underestimation of *AD* was also raised as a possible explanation for why the geologic moment systematically underestimates instrumental magnitude (moment magnitude, M_w) (appendix E, this report). To estimate the potential scale of underestimation of slip in rupture profiles, an envelope estimate of the displacement was developed. Figure F3 shows the Hector Mine rupture, which had one of the larger discrepancies. On average enveloping the displacement profiles increases the average displacement estimate by about 15 percent (fig. F4). The largest events are seen to have the least change from enveloping because little of their length is mapped in sufficient detail for a 1 to 2 km averaging function to have much effect. Average displacements from enveloping surface ruptures were used in appendix E (this report) in developing *L-AD* and moment-area relations.

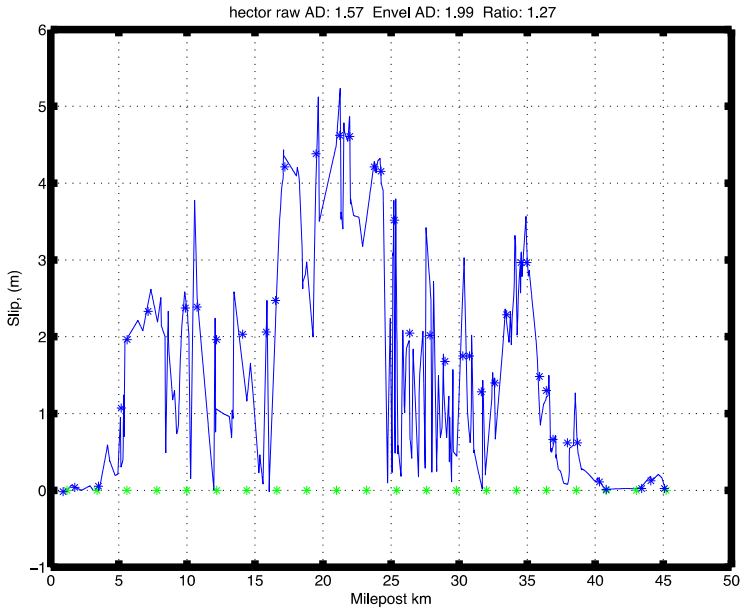

Figure F3. Detailed field measurements of the Hector Mine rupture. *AD* (average surface rupture displacement) using the measurements (rapidly varying line) is 1.57 meter (m). An envelope function was drawn by hand (stars) is used to interpolate assuming a more slowly varying slip function at 1 to 2 kilometer (km) depth. Note that local site conditions can act to hide subsurface motion or less commonly, to amplify it. Average displacement is calculated by summing the trapezoidal area between adjacent points, then dividing by the total rupture length. This approach preserves details where they exist and implements a simple linear extrapolation at all measurement spacings.

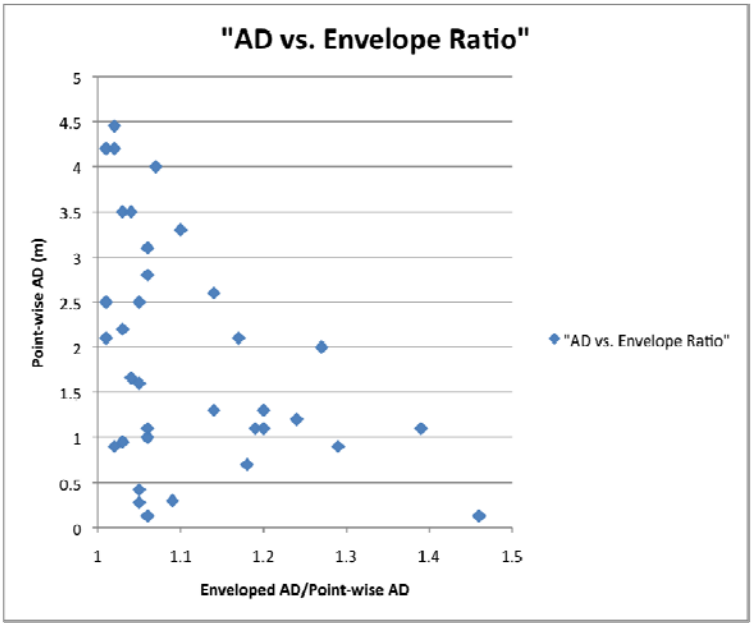

Figure F4. Ratio of enveloped *AD* (average surface rupture displacement) to *AD* for rupture distributions in Wesnousky (2008). Enveloping increases *AD* on average by about 15 percent, but has less effect on longer ruptures because they tend not to be densely sampled along their length. m, meter; vs., versus.

Expanded Event Set

The surface rupture set in Wesnousky (2008) was limited in scope to earthquakes that had both rupture profiles and geologic mapping of nearby fault structures. The goal of that study was to compile data to relate rupture stopping to fault ends, steps, and geometric discontinuities. The uniform presentation of ruptures in the Wesnousky (2008) study made them relatively easy to import and apply to the problem of an average rupture profile shape. Limits on the selection of Wesnousky (2008) events, however, mean that they are potentially incomplete as an event set for developing length versus displacement regressions (appendix E, this report). Recognizing the need for this data in Task E and the overlap with Task F, a wider net was cast to find additional ground ruptures with documented surface rupture measurements.

Two classes of ruptures were given priority for expanding the inventory of surface-rupturing earthquakes. The first were long ruptures that could help constrain shape of the *AD*-*L* curve as the length becomes much longer than width of the seismogenic crust. *AD* and *L* from long ruptures constrain the large event asymptote of the constant stress drop model (appendix E, this report). The second were any ruptures in California that might be developed to constrain the behavior of ruptures in California. These include the 1872 Owens Valley, 1906 San Francisco, and 2010 El Mayor-Cucapah earthquakes and ruptures identified in the new lidar dataset (appendix R, this report). In addition to these priorities, other ruptures were discovered and added as data of opportunity to improve the total set.

Length and *AD* measurements were developed for 25 earthquakes not already in Wesnousky (2008) (table F1; see "Supplement—Description of 25 Earthquakes not in Wesnousky (2008), with Data Sources," which follows the References Cited). Some effort was expended to capture the uncertainties in *L* and *AD*. In many cases the uncertainty in length is not due to measurement uncertainty but reflects other sources such as when the rupture ends were estimated for lack of physical access. Length measures also depend on how significant secondary coseismic ruptures are included. In part for this reason ranges in length and average displacement are inversely related to one another. That is, the maximum estimates for length are associated with minimum estimates for *AD*, normally because the additional length is associated with smaller displacements. The inverse relation between *AD* and length has the positive effect of stabilizing estimates of geologic moment. The combined data are plotted in figure F5. A linear-linear scale is used to make more clear the downward bias for longest ruptures in average displacement relative to the linear increase predicted by Wells and Coppersmith (1994). (The original Wells and Coppersmith (1994) *L*-*AD* relation was developed and provided in log-log space and is shown here strictly for reference.) The added data include reverse faults with average displacements large for their length that contribute to the "scatter plot" appearance. A more detailed analysis of these data and the *L*-*AD* relations recommended for UCERF is provided in appendix E (this report).

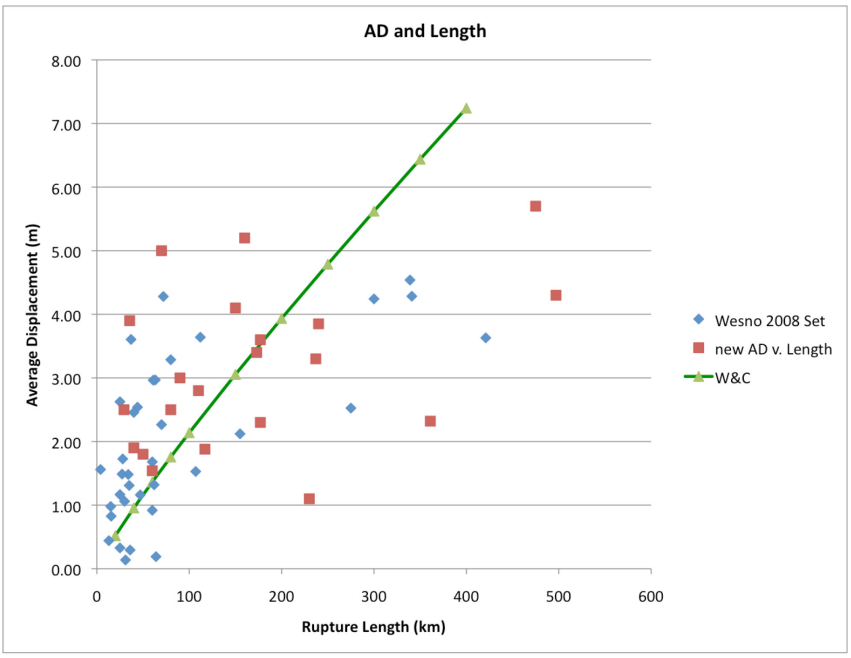

Figure F5. *AD* (average surface rupture displacement) versus length for Wesnousky (2008; "Wesno 2008 Set") and new events ("new AD v. Length"). Green line is Wells and Coppersmith (1994; "W&C"), shown for reference. Earthquakes of all rupture mechanisms are included. m, meters; km, kilometers; v., versus.

Length and (or) average displacement estimates for four earthquakes in Wesnousky (2008) were modified using newer information. For the 1857 Fort Tejon and 2002 Denali earthquakes, new lidar measurements were used to adjust the rupture profile. For the 1857 rupture lidar measurements (Zielke and others, 2010) reduced the displacement estimates in the central part of the rupture. The rupture length was also shortened to remove contributions from the previous 1812 rupture on the southeast. For the Denali rupture lidar measurements were used to fill in displacements across the Denali-Totchunda intersection (Schwartz and others, 2012). Initially it appeared that displacements at the intersection were small, giving the appearance of two nearly separate ruptures, but lidar data show that displacements were quite continuous across this boundary. The 1992 Landers rupture length was reduced and the average displacement slightly increased by removal of the Eureka Peak and Burnt Mountain sections. Ground rupture on these sections was triggered by the main shock and occurred tens of seconds after it (Hough, 1994).

Magnitudes for the compilation are M_w, generally from the latest available studies, unless marked otherwise. Geologic moment magnitudes were not used because of the circularity of using them subsequently to evaluate magnitude-length and magnitude-area regressions. Many early estimates of magnitude especially in the first half of the 20th century were extremely high compared to later estimates, primarily because they relied on surface or shear waves well beyond the free period of the sensors. To the extent possible these estimates were replaced with later M_w values. The Engdahl and Villasenor (2002) M_w estimates were adopted for many events. They developed regressions to estimate modern M_w from early magnitudes, such as surface wave magnitude (M_s), or surface waves that consider limitations in available measurements and

methods. For some events (for example, 1872 Owens Valley and 1911 Chon Kemin), magnitude uncertainties are large, reflecting the range of apparently credible estimates.

Depth estimates also varied among studies of a given rupture. Aftershock zones were used where available. Where seismologists could provide estimates from waveform modeling or depth phases (for example, 2005 Pakistan), that depth was preferred. A depth greater than 25 km is listed only for the 1905 Mongolian earthquakes. The estimate (40 km best, 30–70 km range) is adopted from waveform modeling (Schlupp and Cisternas, 2007). Although instrumentation at the time was limited, their study was based on on-scale body-wave waveforms recorded well within the instrumental free periods. For many earthquakes the depth dimension is not well known.

Figure F6 shows the strike-slip events from the combined dataset that come from California and the tectonically similar Baja California. This view shows that the AD-L relation has a change in slope around L=100 km, similar to the larger dataset. With fewer data points the uncertainty is larger, but these data do show that an AD-L relation that rolls over with increasing length would reasonably represent all known California ruptures.

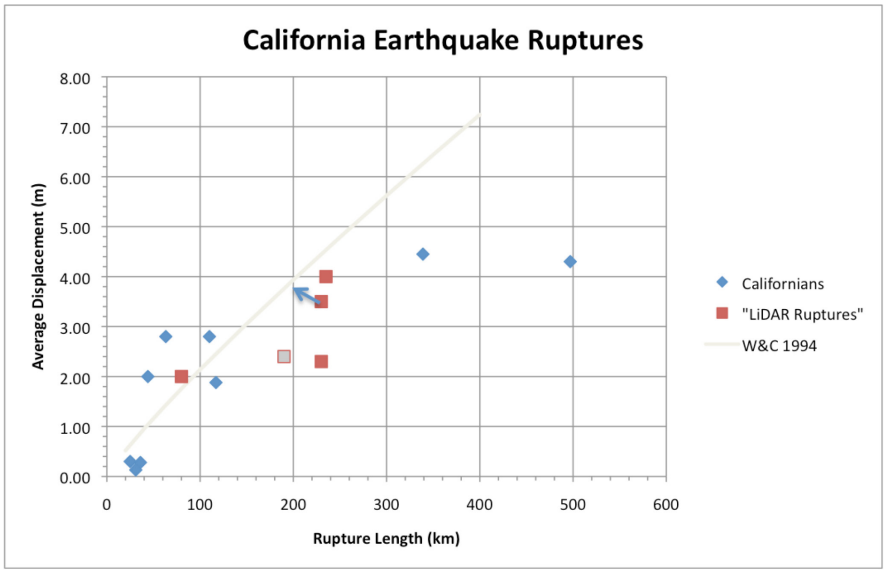

Figure F6. Subset of California earthquakes from figure F4. “Lidar ruptures” are preinstrumental earthquakes for which AD (average surface rupture displacement) and rupture length are known from paleoseismological study and recent lidar measurements. The gray square shows an alternate length for the 1812 rupture if rupture stopped northwest of the Plunge Creek paleoseismic site. Gray line from Wells and Coppersmith (1994; “W&C”) is shown for reference. m, meters; km, kilometers.

The Length Scale for Multi-Fault Ruptures

The *sinesqrt* shape is seen to reasonably represent normalized slip in earthquake ruptures. For a simple fault trace, a usable rupture may be constructed by using the rupture length to scale the shape using a length-average displacement relationship.

For cases where rupture jumps from one fault to another, displacement might be distributed in a couple of ways. The two ways reflect different possible ways that faults link in a multi-fault rupture. One way is to use the complete rupture length, which would scale to a larger *AD*, then distribute slip onto the linking fault sections in a way that makes the total slip add up.

This method in effect views the total slip as the result of a similarly scaled stress field capable of larger slips. A second way is to view fault-to-fault rupture as a sequential triggering process where component faults are loaded individually and produce fault-to-fault ruptures when one happens to trigger the next. In this situation, slip on the participating faults would scale with the individual fault lengths.

To address how slip scales in fault-to-fault ruptures, slips in Wesnousky (2008) strike-slip ruptures are plotted versus their full rupture lengths in figure F7. The regression of Wells and Coppersmith (1994) is also shown. Most events plot around the regression, indicating that the full rupture length and *AD* correspond reasonably. If the same ruptures are divided at step-overs into individual fault ruptures (fig. F8, left), the average displacement on the component faults, perhaps not surprisingly, do not scale with their individual lengths. This means that although fault elements of a fault-to-fault rupture may occasionally be individually loaded in scale with their lengths and trigger sequentially, this situation would be the exception and not the rule. Similar conclusions apply to the non-strike-slip ruptures in Wesnousky (2008) (fig. F8, right). The sequential triggering model might be modified to include dynamic effects. In this model once the second fault is triggered, a feedback condition results in which slip on the first fault increases because the second fault is also slipping. Willemse and others (1996) show with quasi-static models that fault interaction does increase slip but that the increase is relatively small and on the order of 10 to 20 percent. The dynamic interaction model requires information at the leading edge of the rupture to somehow feed back to the successive sections behind. Dynamic models of multi-segment ruptures by Kase (2010) indicate that *AD* does depend on how a rupture is segmented but that slip does not continue to increase with rupture length as the sequential model would predict. However, this question is resolved, the empirical data indicate that full rupture length is most relevant for *L-AD* scaling of model displacements.

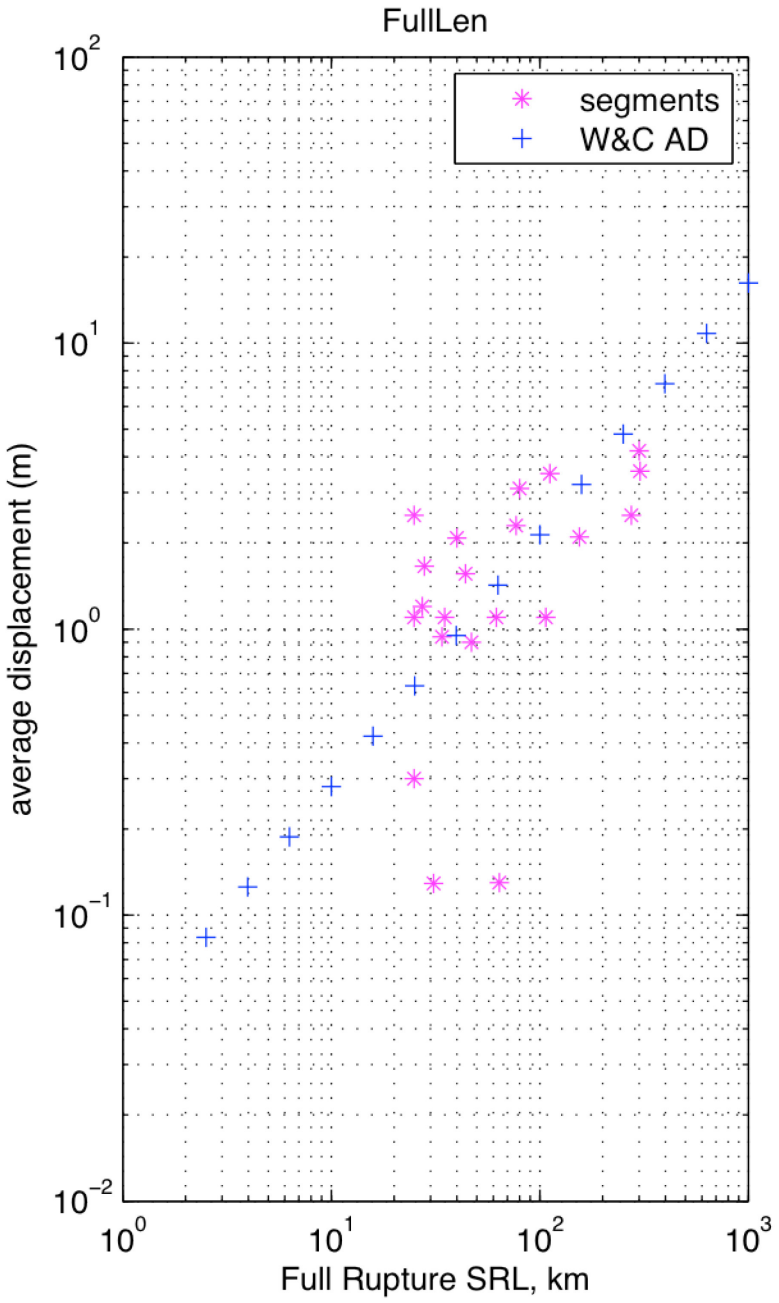

Figure F7. Average surface rupture displacement (*AD*) from Wesnousky (2008) is plotted versus surface rupture length (SRL) for strike-slip ruptures. Length-Average displacement data for Wesnousky (2008) events are consistent in their trend and scatter with the original *L-AD* data of Wells and Coppersmith (1994) (W&C AD). m, meters; km, kilometers.

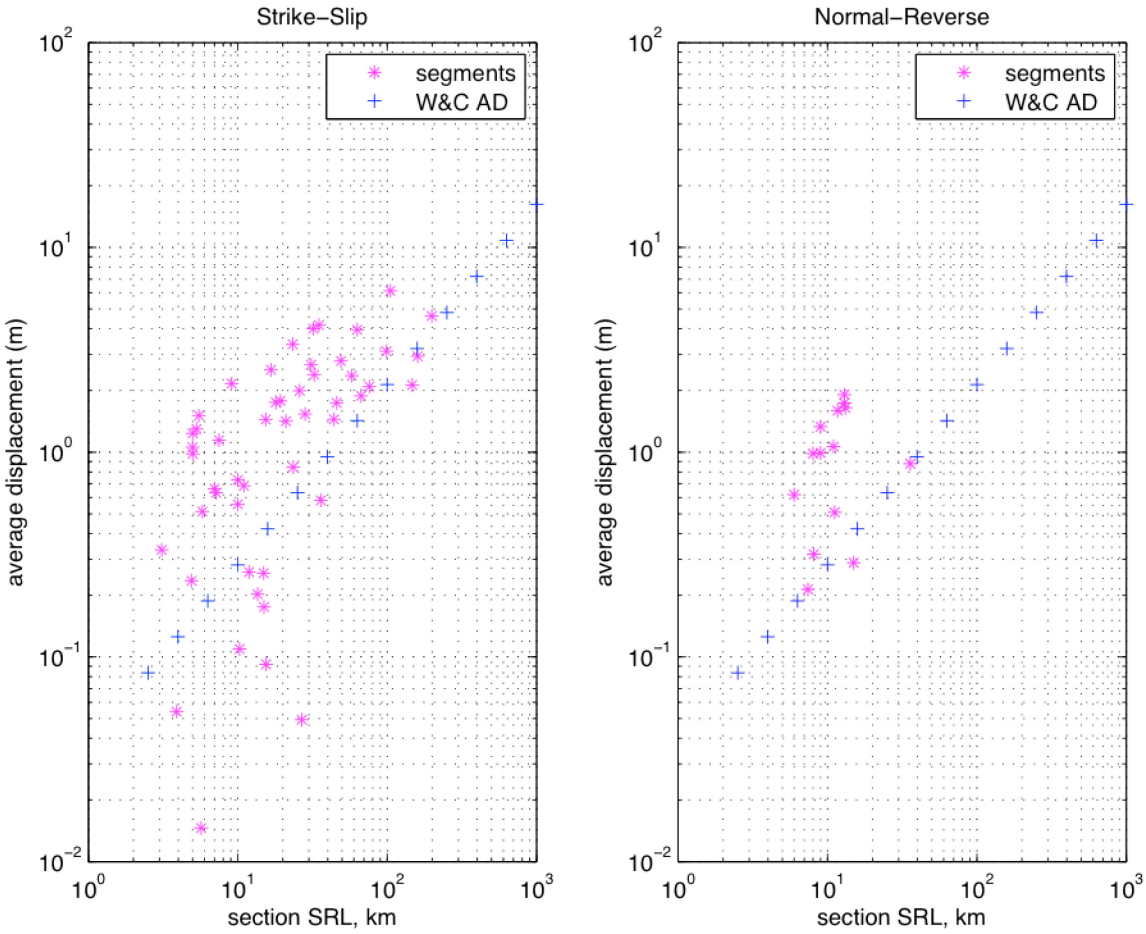

Figure F8. Left, *AD* (average surface rupture displacement) versus *SLR* (surface rupture length) for segments of Wesnousky (2008) strike-slip ruptures. Segment *AD* consistently is greater than would be predicted by the segment length indicating that multi-fault ruptures are not simply individual faults that happen to trigger each other. Right, limited reverse and normal faulting data show a similar pattern. "W&C AD": *AD* data of Wells and Coppersmith (1994); m, meters; km, kilometers.

Slip Distribution at Steps and Fault-to-Fault Jumps

Slip on ruptures such as the 1992 Landers event are seen to end on one fault and continue on another. The individual sections of the rupture have tapered ends suggesting that they should be represented by separate equation-1-like shapes. However, in spite of tapers at steps the net shape of the rupture is similar to a rupture without steps. Slip increases in the middle of the contributing segments of the rupture and tapers more rapidly where they overlap. Thus, when displacement is totaled, the net *AD* is generally consistent with the length. Modeling results (Kase, 2010) indicate that *AD* should be larger for ruptures comprised of fewer, longer contributing segments. However, the differences are small compared to the variability in the empirical *AD* versus *L* data, which includes data from short and long multi-segment ruptures. Future research may allow some reduction in uncertainty in the *AD* versus *L* relation if a systematic effect of segment length can be demonstrated. For UCERF3 use the recommended strategy is to use the *sinesqrt* shape and scale it based on its length with an *L-AD* relation and its uncertainties.

We investigated whether the empirical data indicate that changes in slip direction or rake angle affect surface rupture displacements in a way that could be used with a master shape applied to ruptures. Intuitively, displacement might decrease after negotiating a change in trend or jump to a different style of faulting. However, we found too few clearly documented cases in the empirical data of mapped ruptures to use this information prescriptively in UCERF3.

Applying the Model Rupture Shape

The *sinesqrt* function is continuous, whereas the ruptures in the inversion are discretized into subsections, each of which has constant slip within it. Subsection lengths are constructed to be half the thickness of the seismogenic crust, which varies spatially. Constant slip within subsections leads to a coarse discretization of rupture profiles. To discretize individual ruptures on a single fault, the *sinesqrt* shape is implemented by averaging displacement of the functional form within the section. For a rupture of N sections (N>=2), there are N+1 edges of sections. The value of the functional form is found at each edge. The unnormalized section displacement is the average of the two edge points. The average displacement for the full rupture is implemented by scaling the section average displacements higher or lower using an *L-AD* relation to achieve the desired average for the entire rupture.

References Cited

Biasi, G.P., and Weldon, R.J., 2006, Estimating surface rupture length and magnitude of paleoearthquakes from point measurements of rupture displacement: Bulletin of the Seismological Society of America, v. 96, p. 1612–1623.

Cowie, P.A., and Scholz, C.H., 1992, Physical explanation for the displacement-length relationship of faults using a post-yield fracture mechanics model: Journal of Structural Geology, v. 14, p. 983–997.

Engdahl, E.R., and Villasenor, A., 2002, Global seismicity—1900–1999, *in* Lee, W.H.K., Kanamori, H., Jennings, P.C., and Kisslinger, C., eds., The international handbook of earthquake engineering and seismology: Academic Press, p. 665–690.

Eschelby, J.D., 1957, The determination of the elastic field of an ellipsoidal inclusion, and related problems: Proceedings of the Royal Society of London, v. A, no. 241, p. 376–396.

Field, E.H., and Page, M.T., 2011, Estimating earthquake-rupture rates on a fault or fault system: Bulletin of the Seismological Society of America, v. 101, p. 79–92.

Haeussler, P.J., Schwartz, D.P., Dawson, T.E., Stenner, H.D., Lienkaemper, J.J., Sherrod, B., Cinti, F.R., Montone, P., Craw, P.A., Crone, A.J., and Personius, S.F., 2004, Surface rupture and slip distribution of the Denali and Totchunda faults in the 3 November 2002 *M* 7.9 earthquake, Alaska: Bulletin of the Seismological Society of America, v. 94, no. 6B, p. S23–S52.

Hemphill-Haley, M.A., and Weldon, R.J., II, 1999, Estimating prehistoric earthquake magnitude from point measurements of surface rupture: Bulletin of the Seismological Society of America, v. 89, no. 1264–1279.

Hough, S.E., 1994, Southern surface rupture associated with the *M* 7.3 1992 Landers, California, Earthquake: Bulletin of the Seismological Society of America, v. 84, p. 817–825.

Ingraffea, A.R., 1987, Theory of crack initiation and propagation in rock, *in* Atkinson, B.K., ed., Fracture mechanics of rock: London, Academic Press, p. 71–110.

Kase, Y., 2010, Slip-length scaling law for strike-slip multiple segment earthquakes based on dynamic rupture simulations: Bulletin of the Seismological Society of America, v. 100, p. 473–481.

Langbein, J., Murray, J.R., and Snyder, H.A., 2006, Coseismic and initial postseismic deformation from the 2004 Parkfield, California earthquake observed by Global Positioning System, electronic distance meter, creepmeters and borehole strainmeters; Bulletin of the Seismological Society of America, v. 96, p. S304–S320, doi:10.1785/0120050823.

Okubo, P.G., and Dieterich, J.H., 1984, Effects of fault properties on frictional instabilities produced on simulated faults: Journal of Geophysical Research, v. 89, p. 5817–5827.

Martel, S.J., and Pollard, D.D., 1989, Mechanics of slip and fracture along small faults and simple strike-slip fault zones in granitic rock: Journal of Geophysical Research, v. 94, p. 9417–9428.

Schwartz, D.P., Haeussler, P.J., Seitz, G.G., and Dawson, T.E., 2012, Why the 2002 Denali fault rupture propagated onto the Totschunda fault—Implications for fault branching and seismic hazards: Journal of Geophysical Research, v. 117, no. B11, 304 p.

Shaw, B.E., 2011, Surface slip gradients of large earthquakes: Bulletin of the Seismological Society of America, v. 101, p. 792–804, doi:10:1785/0120100053.

Schlupp, A., and Cisternas, A., 2007, Source history of the 1905 great Mongolian earthquakes: Geophysical Journal International, v. 169, p. 1115–1131.

Vermilye, J.M., and Scholz, C.H., 1998, The process zone—A microstructural view of fault growth: Journal of Geophysical Research, v. 103, p. 12223–12237.

Wells, D.L., and Coppersmith, K.J., 1994, New empirical relationships among magnitude, rupture length, rupture width, rupture area, and surface displacement: Bulletin of the Seismological Society of America, v. 84, p. 974–1002.

Wesnousky, S.G., 2008, Displacement and geometrical characteristics of earthquake surface ruptures—Issues and implications for seismic-hazard analysis and the process of earthquake rupture: Bulletin of the Seismological Society of America, v. 98, p. 1609–1632.

Willemse, E.J., Pollard, D.D., and Aydin, A., 1996, Three-dimensional analysis of slip distributions on normal fault arrays with consequences for fault scaling: Journal of Structural Geology, v. 18, p. 295–309.

Wilkins, S.J., and Schultz, R.A., 2005, 3-D cohesive end-zone model for source scaling of strike-slip interplate earthquakes: Bulletin of the Seismological Society of America, v. 95, p. 2232–2258.

Zielke, O., Arrowsmith, J.R., Ludwig, L.G., Akciz, S.O., 2010, Slip in the 1857 and earlier large earthquakes along the Carrizo Plain, San Andreas fault: Science, v. 327, p. 1119–1122, doi:10.1126/science.1182781.

Table F1. Earthquake rupture parameters for length-average displacement analysis.

[Events are from Wesnousky (2008); parameters from that study with revisions explained in the supplement. "New or post-dating Wesnousky 2008," earthquakes listed under this spanner either predate 2008 but were not included in Wesnousky (2008) or are earthquakes that post-date that compilation. Rows in blue indicate values modified from that study. Ave Displ is average rupture displacement; Lmin, L, and L are minimum, best estimate, and maximum estimated rupture lengths, respectively, in kilometers (km). Dmin, Davg, and Dmax are minimum, average, and maximum average rupture displacements, respectively, in meters (m). Envelope factor is the fraction by which average displacement is increased when the displacement profile is enveloped. Zmin, Z, and Zmax are minimum, nominal, and maximum coseismic rupture depths, respectively, in km. Mmin, M, and "Mmax" are minimum, nominal, and maximum estimates, respectively, of earthquake magnitude. Dip low, dip and dip high are the shallowest, nominal, and steepest dip estimates for the rupture, respectively, in degrees from horizontal. Entries under "Type" refer to the sense of motion on the fault. SSR, strike-slip, right-lateral; SSL, strike-slip, left-lateral; SSL/R is SSL with a reverse component; N/## is normal slip, where present, ## is the nominal dip angle in degrees from horizontal; R/## is reverse slip, where present, ## is the nominal dip angle; NSSR is dominantly normal slip, but with a right-lateral strike-slip slip component; SSN is strike-slip with a normal slip component. SAF, San Andreas Fault; MRE, most recent event. Lettered footnotes are given at the end of the table]

Date	Event	Type	Length (a)	Ave Displ (a)	M_w	L min	L (km)	L max	D min	Davg (m)	D max	Envelope factor (g)	Z min	Z (km)	Z max	M_{min}	M	M_{max}	dip low	dip (deg)	dip high	Note
Wesnousky 2008																						
01/09/1857	Fort Tejon	SSR	339	4.45	7.9	330	339	345		4.45		1.02		15			7.9		85	90	95	(b)
05/03/1887	Sonora	N/60	70	2.2	7.2							1.03										
10/28/1891	Neo-Dani, Japan	SSL	80	3.1	7.3							1.06										
08/31/1896	Rikuu, Japan	R/45	37	3.5	7.2							1.03										
10/02/15	Pleasant Valley, NV	N/45	61	2.6	7.3							1.14										
11/02/30	Kita-Izu, Japan	SSL	35	1.1	6.7							1.19										
12/25/39	Erzincan, Turkey	SSR	300	4.2	7.7							1.01										
05/19/40	Imperial, CA	SSR	60	1.6	6.9							1.05										
12/20/42	Erbaa-Niksar, Turkey	SSR	28	1.66	6.8							1.04										

Date	Event	Type	Length (a)	Ave Displ (a)	M_w	L min	L (km)	L max	D min	Davg (m)	D max	Envelope factor (g)	Z min	Z (km)	Z max	M_{min}	M	M_{max}	dip low	dip (deg)	dip high	Note
11/26/43	Tosya, Turkey	SSR	275	2.5	7.6							1.01										
09/10/43	Tottori, Japan	SSL	10.5	0.6	6.3																	
02/01/44	Gerede-Bolu, Turkey	SSR	155	2.1	7.4							1.01										
01/31/45	Mikawa, Japan	R/30	4	1.3	6.2							1.2										
12/16/54	Fairview Peak, NV	NSSR/60	62	1.1	7							1.2										
12/16/54	Dixie Valley, NV	N/60	47	0.9	6.8							1.29										
08/18/59	Hegben Lake, MT	N/50	25	2.5	7							1.05										
07/22/67	Mudurnu, Turkey	SSR	60	0.9	6.7							1.02										
04/08/68	Borrego Mntn, CA	SSR	31	0.13	6.1							1.06										
02/09/71	San Fernando, CA	R/45	15	0.95	6.7							1.03										
06/02/79	Cadoux, Australia	R/35	10	0.6	6.1																	
10/15/79	Imperial Valley, CA	SSR	36	0.28	6.3							1.05										
10/10/80	El Asnam, Algeria	R/50	27.3	1.2	6.7							1.24										
07/29/81	Sirch, Iran	SS/69	64	0.13	6.4							1.46										
10/28/83	Borah Peak, ID	N/45	34	1.3	6.9							1.14										

Date	Event	Type	Length (a)	Ave Displ (a)	M_w	L min	L (km)	L max	D min	Davg (m)	D max	Envelope factor (g)	Z min	Z (km)	Z max	M_{min}	M	M_{max}	dip low	dip (deg)	dip high	Note
03/03/86	Marryat, Australia	R/35	13	0.42	5.9							1.05										
03/02/87	Edgecumbe, NZ	N/60	15.5	0.7	6.3							1.18										
11/23/87	Super. Hills,CA	SSR	25	0.3	6.2							1.09										
01/22/88	Tennant Crk, Australia	R/45	30	1	6.6							1.06										
07/16/90	Luzon, Philippines	SSL	112	3.5	7.6							1.04										
06/28/92	Landers, CA	SSR	63.2	2.8	7.2		63.2			2.8		1.06										(c)
03/14/98	Fandoqa, Iran	SSN/54	25	1.1	6.6							1.06										
08/17/99	Ismit, Turkey	SSR	107	1.1	7.1							1.39										
10/16/99	Hector Mine, CA	SSR	44	2	6.9					2		1.27										(d)
09/21/99	Chi-Chi, Taiwan	R/70	72	4	7.4							1.07										
11/12/99	Duzce, Turkey	SSR	40	2.1	7							1.17										
11/14/01	Kunlun, China	SSL	421	3.3	7.8							1.1										
11/14/01	Kunlun2, China Spot	SSL	428	2.4	7.8							1.17										
11/03/02	Denali, AK	SSR	341	4.2	7.9		341		4	4.2	4.4	1.02	12	12	15		7.9		80 40	90 48	100 60	(e) (f)

Date	Event	Type	Length (a)	Ave Displ (a)	M_w	L min	L (km)	L max	D min	Davg (m)	D max	Envelope factor (g)	Z min	Z (km)	Z max	M_{min}	M	M_{max}	dip low	dip (deg)	dip high	Note
10/23/04	Mid-Niigata, Japan	R	1	0.1																		
09/28/04	Parkfield, CA	SSR	0.4	0.05																		
												New or post-dating Wesnousky 2008										
03/26/1872	Owens Valley	SSR	110	2.8	7.5	107	110	140	2.6	2.8	3.4		15	17.5	20	7.4	7.5	7.7	65	80	105	
07/23/05	Bulnay, Main trace	SSL			8.4	350	375	395	6.5	6.5	6.7		30	40	70	8.3	8.4	8.5	84	87	90	
07/23/05	Bulnay, with secondary ruptures	SSL	475	5.7	8.4	450	475	495	5.7	5.7	5.8		30	40	70	8.3	8.4	8.5				
04/06/06	San Francisco, CA	SSR	497	4.3	7.9	483	497	517	3.7	4.3	5		12	15	18	7.7	7.9	8	85	90	95	
01/03/11	Chon-Kemin (Kebin), Kyrgystan	R/60	177	3.6	7.7	169	177	260	3.5	3.6	4.1		20	25	30	7.6	7.7	7.9	50	60	70	
12/16/20	Haiyuan, China	SSL	237	3.3	8.25	220	237	260	3	3.3	5			25		8	8.25	8.6	80	90	100	
03/24/23	Luoho-Qiajiao (Daofu)	SSL	80	2.5	7.2	60	80	100	2.3	2.5	3			20			7.2		80	90	100	
08/10/31	Fuyun, China	SSL/R	160	5.2	7.9	160	160	176	4.9	5.2	5.6			20			7.9			90		
01/07/37	Tousuo Lake, China	SSL	150	4.1	7.5	140	150	160	3.2	4.1	4.1			20			7.5		80	90	100	
12/04/57	Gobi-Altai, Main trace	SSL			8.1	240	259	361	3	3.1	4		20	25	30		8.1		45	55	65	

Date	Event	Type	Length (a)	Ave Displ (a)	M_w	L min	L (km)	L max	D min	Davg (m)	D max	Envelope factor (g)	Z min	Z (km)	Z max	M_{min}	M	M_{max}	dip low	dip (deg)	dip high	Note
12/04/57	Gobi-Altai, with major secondary rupture		361	2.32	8.1	259	361	515		2.32							8.1					
04/19/63	Alake Lake, China	SSL	40	1.9	7	30	40	50	1.5	1.9	2.4			20			7		80	90	100	
01/04/70	Tonghai, China	SS	60	1.54	7.2	48	60	90	1.5	1.54	2.1			15			7.2		80	90	100	
02/06/73	Luhuo, China	SSL	90	3	7.4	90	90	105	2.5	3	3.6		12	15	20		7.4		80	90	100	
02/04/76	Motagua, Guatemala	SSL	230	1.1	7.5	230	230	251	1	1.1	1.1		10	15	15		7.5		80	90	100	
05/27/95	Sakhalen Island	SSR	35.5	3.9	7	35	35.5	36	3.8	3.9	4		12	15	18		7		60	70	80	
11/08/97	Manyi, China	SSL	173	3.4	7.5	160	173	180	2.9	3.4	3.7		15	15	24		7.5					
09/27/03	Altai, Mongolia	SSR	50	1.8	7.2	45	50	70	1.5	1.8	2.2		10	12	15		7.2		70	85	90	
10/08/05	Pakistan	R	70	5	7.6		70		4.5	5	5.5			26			7.6		30	39	45	
05/12/08	Wenchuan, China	R/60	240	3.85	7.9	232	240	330	3.48	3.85	4.2		18	20	24		7.9		42	50	60	
	Wenchuan				7.9		312		2.95	3.3							7.9					
04/04/10	El Mayor Cucapah	SSR/N	117	1.88	7.2	115	117	120	1.7	1.88	2.1		9	10	17		7.2		55	65	75	
09/04/10	Christchurch, NZ	SSR	29.4	2.5	7		29.4	31.5	2.4	2.5	2.7		12	15	18		7		67	90	100	
07/09/1905	Tsetserleg, Mongolia (i)	SSL	177	2.3	8	130	177	190	2.3	2.3	3.8		30	40	70	7.8	8	8	55	65	75	

LiDAR-based ruptures																							
Date	**Event**	**Type**	**Length (a)**	**Ave Displ (a)**	M_w	**L min**	**L (km)**	**L max**	**D min**	**Davg (m)**	**D max**	**Envelope factor (g)**	**Z min**	**Z (km)**	**Z max**	M_{min}	M	M_{max}	**dip low**	**dip (deg)**	**dip high**	**Note**
12/1812	1812, SAF	SSR	230	2.3		190	230	270	1.8	2.3	2.8											
	1812 short (h)	SSR					190			2.4												
Circa 1700	1700s, SAF	SSR	230	3.5		210	230	280	2.5	3.5	3.8											
1700's	Clark MRE, San Jacinto fault	SSR	80	2		76	80	85	1.8	2	2.2											
Circa 1690	1690 S. SAF	SSR	235	4		220	235	250	3.5	4	4.5											

Notes:

(a) Column shows best estimates. Blank if the rupture has a significant alternative. See columns to right and accompanying discussion.

(b) Length, *AD* modified using lidar of Zielke and others (2010).

(c) Length reduced, *AD* increased by removing Eureka Peak and Burnt Mountain triggered rupture (Hough, 1994).

(d) *AD* from enveloped rupture profile.

(e) Length increased to include Denali Fault trace north of the Susitna Glacier (Heussler and others, 2004).

(f) Dip of Susitna Glacier Fault.

(g) Multiply D_{avg} by this factor to get enveloped average displacement.

(h) 1812 San Andreas Fault rupture length if rupture stopped NW of the paleoseismic site at Plunge Creek.

(i) Reported Tsetserleg length, average displacement, and instrumental waveform parametric data considered inconsistent; event not recommended for use in regressions.

Supplement—Data Supplements and Modifications to Wesnousky (2008), with Sources

Introduction

The event set used in magnitude-area relations of Hanks and Bakun (2002) differ from the smaller set examined by Wesnousky (2008). At the March 2011 UCERF3 workshop in Menlo Park it was shown that the difference would have consequences for the relationships recommended to UCERF3 for magnitude-area scaling and for a proposed alternative, average displacement (*AD*) versus surface rupture length (*L*) (appendix E, this report). The Wesnousky (2008) events were recognized as well reviewed, but the collection was restricted to events with good mapping of the rupture and nearby faults and was limited in resources for data collection. The Wesnousky (2008) data were not developed to constrain *AD* versus *L* regressions. As a result of the workshop, a review was recommended of the extra events in Hanks and Bakun (2002) and of the literature for any additional events that could improve the *L*-*AD* curve, focusing particularly on events with large rupture lengths.

The list of largest events discussed in the March 2011 workshop included:

- 1872 Owens Valley, California
- 1905 Tsetserleg, Mongolia
- 1905 Bulnay, Mongolia
- 1906 San Francisco, California
- 1911 Chon-Kemin, Kyrgystan
- 1920 Haiyuan, China
- 1976 Motagua, Guatemala
- 1997 Manyi, China
- 2008 Wenchaun, China
- 2010 El Mayor Cucapah, Baja California, Mexico

Other events were discovered in the course of the review with sufficient data to include below. We also examined a few particular parameters in Wesnousky (2008) table F1 where workshop attendees questioned particular entries. The discussion below covers all new events and any Wesnousky (2008) events for which *L*, *AD*, or M_w were modified.

A review of available rupture maps indicates that ruptures sometimes include overlapping and secondary traces that would not be counted in the main trace total length. Events that have overlapping rupture segments that contribute to moment release but not to total rupture length may create a bias in regression of displacement versus rupture length. To provide an idea of how significant this effect could be, an estimate the length with overlaps is provided for a few key events.

Events to Supplement the Wesnousky (2008) Collection

Acronyms used below: SSR, strike-slip, right-lateral; SSL, strike-slip, left-lateral; SSL/R is SSL with a reverse component; N/##, normal slip, where present, ## is the nominal dip angle in degrees from horizontal; R/##, reverse slip, where present, ## is the nominal slip angle; NSSR, dominantly normal slip, but with a right-lateral strike-slip slip component; SSN, strike-slip with a normal slip component.

Owens Valley, California, March 26, 1872

Style: SSR
Length: 110 (107–140) km
AD: 2.8 (2.6–3.4) m
Depth: 17.5 (15–20) km
Dip: 80 (65–105) degrees
Instrumental Magnitude: N/A
Discussion: Beanland and Clark (1994) mapped the rupture in the field and integrated earlier observations. Only a limited number of offsets were obtained because much of the evidence was lost to erosion. Some of the most important reported displacements are internally inconsistent (for example, 6.1 m of strike-slip on a trace a few hundred meters long). The length estimate of 110 (107–140) km uses the early known length of 90 km plus an accepted extension from low-angle sun photos by Vittori and others (2003) to the southern end of Owens Lake, plus 3 km for trace lost over time. One meter strike slip and 0.5 m of normal offset are added to the *AD* calculation to give the southern 8.7 km of extension enough displacement to be visible in low angle sun photographs taken decades after the event. Upper bound length is from Hough and Hutton (2008); if used, *AD* would decrease as surface rupture, if present, was apparently small. The *AD* computed for horizontal component offset, 2.6 m, is from lidar observations (appendix R, this report). The *AD* estimate in table F1 combines 2.6 m horizontal with 1 m average vertical displacement from Beanland and Clark (1994) using the square-root of sum of squares. Depth is averaged from double-difference relocations of Hauksson and Shearer (2005), as cited in Hough and Hutton (2008). Dip is from Beanland and Clark (1994). No instrumental magnitude exists; Hough and Hutton estimate *M* 7.6–7.8 from intensity measures and comparison with the 1906 earthquake.

Tsetserleg, Mongolia, July 9, 1905

Style: SS Left Oblique
Length: 177 (130–190) km
AD: 2.3 (2.3–3.8) m
Depth: 40 (30–70) km
Dip: 65 (55–75) degrees
Instrumental Magnitude: M_w 8.0
Discussion: The 1905 Tsetserleg earthquake was reviewed using data from Baljinnyam and others (1993) and Schlupp and Cisternas (2007). The few mapped displacements for the July 9, 1905, Tsetserleg earthquake were relatively small—2 m or less—but averaged to 2.3 m by Baljinnyam and others (1993). Upper *AD* estimate is 3.78 m, calculated by adding 2.3 m of displacement ×130 km of mapped rupture length plus 6 m average displacment over 60 km of rupture length inferred from waveform modeling. The nominal rupture length of 177 km is from Vergnollee and others (2003) and weights instrumental results. The minimum length of 130 km is from geologic mapping; maximum=190 km, from waveform modeling. Dip from mapping is 65 ±10 degrees over 80 km and subvertical in the southern 50 km where it approaches the Bulnay rupture. Depth 40 (30–70) km is from waveform modeling, weighting the Bulnay rupture results

where it is better resolved. The Richter (1958) magnitude estimate (*M* 8.4) would have used clipped body waves or surface waves well beyond the free period of available sensors. The Schlupp and Cisternas (2007) magnitude estimate, M_w 8.0, used waveform modeling of portions of on-scale instrumental records within their free periods, with a clear source-time function 65 seconds (s) long and a fitting-based rupture length of 190 km. The preferred magnitude includes a 60 km extension beyond the mapped end of the rupture with an average displacement of 6 m. There is conventional satellite evidence for a continuing rupture, but field confirmation and measurement of this additional rupture section has not been reported. The majority of the Tsetserleg earthquake seismic moment release thus occurred where surface rupture has not been confirmed. The extra moment would create a major difference between the geologic and instrumental magnitudes. The event is listed in table F1, but not recommended for use in *AD-L* or magnitude-area relations.

Bulnay, Mongolia, July 23, 1905

Style: SSL
Length: 375 (350–395) km main trace; 475 (450–495) km with major secondary traces
AD: 6.5 (6.5–6.7) m, main trace only; 5.7 (5.7–5.8) m with secondary traces
Depth: 40 (30–70) km
Dip: 87 (84–90) degrees
Instrumental Magnitude: M_w 8.4 (8.3–8.5)
Discussion: The July 23, 1905, Bulnay rupture has multiple displacement measurements from field mapping in 1914 through 1991, plus spot checks of offsets by U.S. Geological Survey (USGS) personnel (Schwartz and others, 2009). Photographic evidence clearly shows that offsets from this event were very large. The surface rupture and moment release for this event apparently included significant secondary ruptures that contributed to the total seismic moment.

The main trace is 375 (350–395) km long centered on the estimate from Baljinnyam and others (1993). The upper estimate includes minor secondary traces from mapping. The lower length estimate is from D. Schwartz (written commun., 2011). USGS field work did not confirm either end of the main trace.

Major secondary ruptures occurred on the Teregtiyn and Dungen Faults; these ruptures total about 100 km in length. The Teregtiyn rupture is 80 km long, 20 km with 3.2±1 reverse faulting on a 50–70 degree northeast-dipping plane, and 60 km of en-echelon faults, with 3.0±1 m strike-slip offset. The association of the Teregtiyn rupture with the main Bulnay rupture is strongly suggested from modeling of horizontal component seismograms that require significant moment release at a high angle to the main rupture trace. The evidence against it being coseismic with the Bulnay main rupture is primarily from silence, it not being mentioned in Russian fieldwork from 1914 and only first reported in 1959. The Dungen rupture is 20-22 km in length, and estimated to have 1.5±0.5 m slip on a vertical plane. Many other shorter scarps were recognized in the field but not included in the summary mapping. With principal secondary structures the rupture length is 475 (450-495) km. This is considered the most representative length for the 1905 Bulnay rupture.

AD was developed from the rupture profile displacement measurements of Baljinnyam and others (1993) and D. Schwartz (written commun., 2011; Schwartz and others, 2009). Where measurements disagreed, later work that included USGS personnel was used. Average displacement estimates use linear extrapolation between field measurements, and linear extension to the ends of the fault. The average displacement on the main trace is 6.7, 6.5, and 6.5 m for 350, 375, and 395 km lengths, respectively. With the secondary traces, *AD* estimates are 5.8, 5.7, and 5.7 m, for 450, 475, and 495 km total trace lengths. The secondary ruptures would increase the total estimated seismic moment by about 11 percent.

Dip is from Schlupp and Cisternas (2007). Main trace dips are well constrained by the seismic data and differ by about a degree between the west and east sections of the main trace.

Depth: Estimate of 40 km is adopted from Schlupp and Cisternas (2007, p. 1128) based on waveform modeling and comparison with the (relatively) nearby 2001 Kokoxili (Kunlun) earthquake. For the main trace, fault rupture depths from 30 km to 70 km lead to reasonable waveform fits.

Magnitude: Source-time function was 120 s. Waveform fits give M_o=3.97×10^{21} to 7.27×10^{21} N*m (Newton-meter), M_w 8.34 to 8.51; table values M_w 8.4 (8.3–8.5) reflect realistic precision. Earlier, larger magnitude estimates using M_s or surface waves (for example, Richter, 1958) rely on instrument corrections well beyond the free period of the sensors.

San Francisco, California, April 18, 1906

Style: RL SS
Length: 497 (483–517) km
AD: 4.3 (3.7–5.0) m
Depth: 15 (12–18) km
Dip: 90 (85–95) degrees
Instrumental Magnitude: M_w 7.9 (7.8–8.0)
Discussion: The primary resources for study of the full rupture profile are Thatcher and others (1997), Wald and others (1993), and Song and others (2008). Thatcher and others (1997) invert survey-based geodetic data, with some lines not resurveyed until substantially after 1906. Their rupture profile ends to the northwest at Shelter Cove with 8.5 meters of slip and no controls north of that point. Geodetic offsets south of San Francisco are generally 1 to 2 m larger than point offset measurements in the Lawson (1908) report. Wald and others (1993) attempted to invert the few available seismic records for a slip distribution. Sensor bandwidth limitations prevented their estimate from being widely accepted. Song and others (2008) conducted a joint inversion of seismic and geodetic data. Their estimate is considered here as most reliable.
Length of 497 (483–517) km is based on the documented surface rupture (477 km) plus a taper from 6 m to 0 on the north end at a taper rate of 3.3×10^{-3}/km (3.3 m per km), twice the steepest internal taper of the Song and others (2008) model. The lower L estimate tapers from 6 m to 0 at 10^{-3}/km; the upper L estimate tapers at 6.7×10^{-3} and extends the rupture to the Mendocino Triple Junction. Average displacement is from the Song and others slip profile, with linear tapers on the ends described above. Uncertainties assigned

at ±15 percent. Depth of rupture assigned at 15 ± 3 km, corresponding to a 20 percent uncertainty. Magnitude is from Song and others (2008) with 0.1 unit uncertainties.

Chon-Kemin, Kyrgyzstan, January 3, 1911

Style: R60
Length: 177 (169–260) km
AD: 3.6 (3.5–4.1) m
Depth: 25 (20–30) km
Dip: 60 (50–70) degrees
Instrumental Magnitude: M_w 7.7 (7.6–7.9)
Discussion: This earthquake is characterized by major reverse faulting on multiple subparallel strands. The surface rupture was studied shortly after it occurred in a major Russian field effort. Recent field investigations by Arrowsmith and others (2005) and Crosby and Arrowsmith (written commun., 2013) focused on the surface rupture and on separating the 1911 rupture from earlier ruptures.

The length of 177 km was obtained by digitizing the rupture map in Arrowsmith and others (2005), generalizing the rupture as two simple strands with ~8 km overlap. Minimum length of 169 km subtracts 8 km where the strands overlap. The maximum length, 260 km, includes the more significant subparallel secondary strands. Average displacement of 3.6 m is based on Arrowsmith and others (2005) estimates of the displacement made on individual reaches of the fault, with linear connections where they have gaps in their displacement profile. *AD* range is 3.5 to 4.1 m. The displacement estimate at 260 km length assumes 160 km×3.6 m plus 100 km×1.5±0.5 m averaged over 260 km, or 2.8 (2.6–3.0) m. The average displacement of 1.5±0.5 m for the secondary rupture displacement is based on it being large enough to be evident for reconnaissance mapping while still secondary to the main traces.

The depth of 25±5 km is the down-dip extent is based in seismicity extending to 20 km vertical depth. Average dip is ~60 degrees from Crosby and Arrowsmith (written commun., 2013) mapping, ±10 degrees based on their narrative description and geometric considerations for projecting faults to depth.

Engdahl and Villesenor (2002) recalibrated historic instrumental magnitude methods and estimate M_w 7.8 for the Chon-Kemin earthquake. This agrees reasonably with the geologic moment of Arrowsmith and others (2005), M_o=3.86e+20, and M_w 7.72. The range of M_w is estimated from the relative consequences of varying geometric uncertainties around M_w 7.7.

Haiyuan, China, December 16, 1920

Style: SSL, SSLO
Length: 237 (220–260) km
AD: 3.3 (3.0–5.0) m
Depth: 25 km
Dip: 90 (80–100) degrees
Instrumental Magnitude: M_w 8.25 (8.0–8.6) See discussion.

Discussion: This rupture occurred on the Haiyuan (Nanxihuashan) Fault Zone.
Length: The Dec 16, 1920 Haiyuan earthquake was 237 km long, adopted from Liu-Zeng and others (2007). Mapping that would permit estimation of off-fault and secondary ruptures was not available.

Deng and others (1986) present displacements measured at 168 points along the central ~170 km of the rupture. Rupture was primarily left lateral and left oblique, with most sections of the fault trending 10 to 15 degrees northwest of the net slip of the main trace. Pull-apart structures developed in several left steps between sections, presumably to accommodate this obliquity. Deng and others (1986) give strike-slip displacement averages by fault segment. Most averages are over 10 or more measurements, with a few likely outliers removed. Strike-slip measurements were made on cultural structures (for example, walls) and some small gullies.

The western ~60 km was not mapped by Deng and others (1986), so for this part of the rupture displacement was assigned at the level of the westernmost displacements. Small tapers were applied to the ends, at a rate of 5×10^{-4} (0.5 m per km). The Deng and others (1986) report a length of 220 km, with ~10 km uncertainty in the western end and an inequality length given for the eastern-most section. Additions on each end, consistent with the uncertainties in their estimate, bring the total to 237 km. Deng and others (1986) do not give displacement values for one section, SF7 (12 km length). A displacement of 2 m was assigned based on the argument that it was large enough to make the section mappable. Displacements in tensile-shear basins totaled at least 30.5 km. The authors state that off-fault displacements could have been missed. For the minimum *AD*, we replace the western 60 km assigned displacements of 2 m with 1.0 m: (237 km×3.3 m–60 km×2 m+60 km×1 m)/237 km=3.0 m *AD*.

Using the Deng and others average displacements and section lengths modified as described above gives an average rupture displacement of 3.28 m for the main trace of 237 km length. Including normal faulting in pull-aparts and overlaps gives *L*=268 and *AD*=3.32 m. The average depends somewhat on displacements assigned to the western unmapped region. An upper estimate of 5.0 m allows for 50 percent of the rupture being unrecognized, either being off the main trace or otherwise obscured by landslides or erosion. Even with these allowances the *AD* estimates here are relatively low compared with other values ascribed to this rupture.
Depth of seismicity: 25 km, from Engdahl and Villasenor (2002). Dip was subvertical.
Magnitude: Magnitude estimates for this earthquake vary widely. The magnitude in table F1 is M_w 8.25 (8.0–8.6). Engdahl and Villasenor (2002) list it at M_w 8.3 using their recalibrations. Chen and Molnar (1977) give $M_o=3.0\times10^{28}$ dyne-centimeter based on a 200 km rupture and 10 m slip (M_w=8.25). Liu-Zeng and others (2007) cite *M* 8.6. Klinger (2010) lists M_s=8.0, which may understate the M_w because M_s is estimated at a 20 s period and thus could be saturated.

Luoho-Qiajiao (Daofu), China, March 24, 1923

Style: SSL
Length: 80 (60–100) km
AD: 2.5 (2.3–3.0) m
Depth: 20 km

Dip: 90 (80–100) degrees
Instrumental Magnitude: M_w 7.2
Discussion: Rupture was on the Xianshuihe Fault. Allen and others (1991) refer to this as the Sharato earthquake. Papadimitriou and others (2004) surveyed measurements in the central part of the rupture, nominally near the maximum offsets. Their observations of rice paddy offsets, tree lines, produced generally high-quality measurements. Coauthor Weldon participated in this study. Papadimitriou and others (2004, p. 1693) use 3 m as an average, based on measurements of 2.3 to 4.2 m in the central 10 to 20 km rupture section. Applying a sinesqrt shape with 3 m average across this section and a rupture length of gives an *AD* of ~2.5 m. The minimum *AD* assumes that 3 m in the measured area is the maximum of a sinesqrt shape. The upper *AD* estimate of 3.0 m assumes a maximum of ~4 m and the sinesqrt shape. Our length estimate is 80 (60–100) km. The maximum length of 100 km is from Papadimitriou and others (2004, p. 1695), citing mapping done in 1934. Allen and others (1991) list the rupture length only as ">60 km." The dip is approximately vertical according to Papadimitriou and others (2004). Depth of seismicity is assumed to be ~20 km. Instrumental magnitude of M_w 7.2 (M_o 0.62×10^{20} N*m) is from Papadimitriou and others (2004).

Fuyun, China, August 10, 1931

Style: SSL/R
Length: 160 (160–176) km
AD: 5.2 (4.9–5.6) m
Depth: 20 km
Dip: 90 degrees
Instrumental Magnitude: 7.9
Discussion: This rupture is generally characterized by left-lateral strike slip on a subvertical fault plane. Some oblique slip is indicated by the fault style in the unmapped northwest 40 km of the rupture. Key new data are provided by Klinger and others (2011) from SPOT/Quick Bird satellite imagery, which covers the eastern 120 km of the rupture. Ground-truth values for several offsets were measured in the field. Secondary ruptures on the map of Klinger and others (2011) total 38 km. The rupture length estimate and minimum of 160 km are from Klinger and others (2011). The maximum length of 176 km is 10 percent greater, and similar to the value of 171 km from Vergnolle and others (2003). With secondary traces the potential full length is 160+38=198 km.

Klinger and others (2011) densely sampled displacements of the most recent event (MRE) along the central 110 km of the rupture within the extent of the SPOT data. In the 8 km length from the end of the SPOT data to the southeast end of the rupture, we applied a linear displacement gradient. For the 40 km northwest not covered by SPOT measurements, a tapered end was formed by copying the southeast 40 km and reflecting it. Clearly the actual shape of the northwest 40 km is speculative. Note that the average of 6.2 meters in the central 110 km does not translate directly to 6.2 m for the whole rupture. An *AD* of 5.2 m is found from the net rupture profile. Minimum *AD*=4.9 m is found by replacing the 40 km northwest taper with 2 m constant value. The maximum *AD*=5.6 m is found by replacing 40 km northwest taper with 20 km full amplitude (6.5 m) and 20 km on a linear taper to zero displacement at the rupture end.

The depth of this earthquake is not well known. A focal depth of 19 km is reported in the AGI Map Volume. The depth of 20 km in table F1 is from Vergnolle and others (2003). Magnitude M_w=7.9 is reported in Klinger and others (2011) and Engdahl and Villasenor (2002).

Tuosuo Lake (Dongxi), China, January 7, 1937

Style: LL SS
Length: 150 (140–160) km
AD: 4.1 (3.2–4.1) m
Depth: 20 km
Dip: 90 (80–100) degrees
Instrumental Magnitude: 7.5
Discussion: This rupture is variously called the Tuosuo Lake, Dongxi, or Huashixia earthquake. It ruptured the eastern Kunlun Fault in northern Tibet with nearly pure left-lateral strike slip motion. Most recent published data are in Guo and others (2007). New data in that study include air photos from 1963-1966, field mapping, displacement measurements at 9 locations, and trenching. Displacement sites are distributed along the rupture. The air photos resolve some uncertainties in field studies from the 1980's including the boundary with the 1963 Alake Lake rupture and the (lack of) overlap with the Tuosuo Lake rupture. The magnitude is adopted from Guo and others (2007), citing the International Seismological Centre (2001).

The length of 150±10 km and average displacement of 4.1 m are from Guo and others (2007). The minimum *AD*=3.2 m recognizes that SE displacements are not well known. *AD* max=4.1 m, assessing that the SE displacements are unlikely to increase the average above the Guo and others (2007) estimate. At the March 2011 UCERF3 workshop, Klinger summarized this rupture as M_w 7.5, based on a 15 km seismic width, 120 km length, and average slip of 3 m but did not address why the Guo and others (2007) results should not be accepted. Dip is vertical, with minor variation.

Gobi-Altay, Mongolia, December 4, 1957

Style: SSL
Length: 259 (240–361) km
AD: 3.1 (3.0–4.0) m
Depth: 25 (20–30) km
Dip: 55 (45–65) degrees
Instrumental Magnitude: M_w 8.1
Discussion: The primary source for displacement measurements of the 1957 Gobi-Altay earthquake is Kurushin and others (1997). Ground rupture was mapped in remarkable detail to a distance of several tens of km on either side of the main trace. The 1957 Gobi-Altay rupture main trace is 259 km long with left-lateral strike slip displacements of 3 to 4 m on much of it but locally as much as 5 to 7 m. The average main trace displacement is 3.1 m. This modest average displacement might be anticipated from the table of 46 measured displacements in Kurushin and others (1997)—only two exceeded 5.8 m.

Minimum and maximum *AD*=3.0 m and 4.0 m, respectively, are based on alternative choices of length. *L_min*=240 km discounts minor normal faulting on the east end and reverse structures at the western rutpure termination. This earthquake also included several tens of km of secondary ruptures, many with reverse mechanisms that would have contributed to moment release. Including larger secondary structures, *L_max*=361 (*AD* ~3 m). The mapped displacements of off-main fault rupture extended for ~256 km of the fault length, with an average displacement of 1.5 m. This comes to about half the main trace moment. Length considering all mapped secondary faulting=515 km, with *AD*=2.3 m.

Dip on the main trace=55 degrees from Kurushin and others (1997) field mapping; 10 degree range (45–65) is a generic uncertainty. The dip is remarkable for a primarily strike-slip rupture.

Rupture depth is estimated to be at least 25 km. Adjoining the main trace is a mechanically coherent plateau-like structure some 60 km in length named Il Bogd. A secondary reverse fault rupture skirts much of the way around this structure, but internally it is relatively undeformed, as though rooted at depth. Kurushin and others (1997) used a depth of 20 km in moment estimates. Engdahl and Villasenor (2002) also use depth=25 km with their M_w 8.1 estimate.

Alake Lake, Tibet, April 19, 1963

Style: SSL
Length: 40 (30–50) km
AD: 1.9±0.5 m
Depth: 20 km
Dip: 90 (80–100) degrees
Instrumental Magnitude: M_w 7.0
Discussion: This earthquake produced left-lateral strike slip on the Kunlun Fault west of the 1937 Tuosuo Lake rupture. It is distinguished from the latter and from older ruptures to the west of the 1937 rupture based on the freshness of scarp and surface evidence of faulting in 1963–1966 air photos (Guo and others, 2007). Length: 40±10 km. Displacement: *AD*=1.9 (1.5–2.4) m. Two displacement measurements (1.6±0.5 and 2.3±0.5 m) were taken near the center of the rupture. Rupture depth of 20 km is a default value.

Tonghai, China, 4 January 1970

Style: SSR
Length: 60 (48-90) km
AD: 1.54 (1.54–2.1) m
Depth: 15 km
Dip: 90 (80-100) degrees
Instrumental Magnitude: M_w 7.2
Discussion: Right-lateral slip occurred on the Qujiang Fault, which is part of the Honghe (Red River) Fault system. The rupture length of 60 km is from Hu (2002). Length

minimum of 48 km is from the mapped rupture trace, the maximum=90 km from modeling by Zhou and others (1983). AD=1.54 m from slip measurements in Zhou and others (1983). Upper value *AD*=2.1 m is +20 percent uncertainty, reflecting potential underestimates of geologic offsets. M_w=7.2 is from Engdahl and Villasenor (2002), with rupture depth=14 km.

Luhou, China, February 6, 1973

Style: SSL
Length: 90 (90–105) km
AD: 3.0 (2.5–3.6) m
Depth: 15 (12–20) km
Dip: 90 (80–100) degrees
Instrumental Magnitude: M_w 7.4
Discussion: The Luhou earthquake occurred on the Xianshuihe Fault. Papadimitriou and others (2004) noted several displacement measurements in the central ~10 km of the rupture. They report that the length of 90 km was exceptionally well mapped but give a length of 105 km elsewhere in the paper. *AD* of 4 m in Papadimitriou and others (2004) is considered an overestimate based on field checks by Weldon (unpub. data, 1997). Weldon (unpub. data, 1997) work on this rupture put the central 10 to 15 km at about 4 m. If 4 m is the approximate maximum of a sinesqrt rupture shape, *AD*=4/1.31=3 m as the rupture average (D_{max}/AD=1.31 for the sinesqrt shape). D_{max}=3.6 m from Zhou and others 1983, back calculating from seismic data with depth=20 km. Dip and depth from Papadimitriou and others (2004). Magnitude M_w 7.4 (M_o=1.70×10^{20} Nm) from Engdahl and Villasenor (2002).

Motagua, Guatemala, February 4, 1976

Style: SSL
Length: 230 (230–251) km
AD: 1.1 (1.0–1.1) m
Depth: 15 (10–15) km
Dip: 90 (80–100) degrees
Instrumental Magnitude: M_w 7.5
Discussion: Rupture was almost pure sinistral displacement on a vertical, N. 65° E. to N. 80° E. trending fault. The best estimate length is 230 km, from Plafker (1976) and Bucknam and others (1978). Secondary fault ruptures total 25 km and include the Mixco zone >10 km long with ~13 cm oblique slip, the Villa Linda-Castanas zone ~8 km long, and the Incienso-Santa Rosa at 7 km long. Minimum=230 km. L_max=251 km is obtained by summing the main and secondary traces. Aftershocks and damage span a length of 300 km. The maximum displacement was 3.25 m. *AD*=1.0 m is from the Bucknam and others (1978) rupture profile. The upper *AD* estimate of 1.1 m includes a small amount of afterslip. M_w 7.5 is from Engdahl and Villasenor (2002), with depth=13 km.

Manyi, China, November 8, 1997

Style: SSL
Length: 173 (160–180km)
AD: 3.4 (2.9–3.7) m
Depth: 15 (15–24) km
Dip: 70 (60–80) degrees
Instrumental Magnitude: M_w 7.5
Discussion: This M_w 7.5 earthquake occurred on the western-most Kunlun Fault. The sense of motion was mostly left-lateral strike slip. Three model length and slip estimates were constructed primarily from InSAR (Funning and others, 2007; Wen and Ma, 2010). *AD* and range reflect three InSAR modeled displacements. *AD* agreement among the models is good. Funning and others (2007) show that the aftershock distribution matches the coseismic surface rupture extent.
Depth: 15 km (hypocenter at 15 km). The Peltzer and others (1999) model includes slip down to 20 km depth. D_{max}=24 is from the Engdahl and Villasenor (2002) centroid moment tensor (CMT) depth.
Magnitude: M_w 7.5 is from Wen and Ma (2010). Engdahl and Villasenor (2002) also estimate M_w 7.5.

Sakhalen Island, Russia, May 27, 1995

Style: SSR
Length: 35.5 (35–36) km
AD: 3.9 (3.8–4.0) m
Depth: 15 (12–18) km
Dip: 70 (60-80) degrees
Instrumental Magnitude: M_w 7.0
Discussion: The fault plane dips west at approximately 70 degrees on a trend N. 15° E. on the Gyrgylan'i-Ossoy Fault. Surface rupture length is 35.5 km from Shimamoto and others (1996) mapping. Tight bounds (35–36 km) are assigned because the rupture was mapped promptly by at least two teams of geologists. Shimamoto and others (1996) give a detailed slip distribution of both strike-slip and vertical displacement components. Horizontal average displacement is 3.8 m. Including the vector vertical increases *AD* to 3.9 m. Small uncertainties are estimated (±0.1 m), because the rupture was mapped thoroughly and not long after the earthquake. Dip 70 (60–80) degrees northwest is from Shimamoto and others (1996).

Magnitude was calculated by Katsumata and others (2004). M_o 4.2×10^{19} N*m, and M_w=7.0. Engdahl and Villasenor (2002) estimate M_w 7.1 and a depth of 18 km. The Katsumata and others (2004) study is preferred here because it is more detailed and event specific than the Harvard CMT. A depth of 15 km (±3) is based on aftershock studies from temporary arrays associated with the field work.

Altai, Mongolia, September 27, 2003

Style: SSR
Length: 50 (40–70) km
AD: 1.8 (1.5–2.2) m
Depth: 12 (10–15) km
Dip: 76 (71–82) degrees
Instrumental Magnitude: M_w 7.2
Discussion: Rupture parameters for this right-lateral strike-slip earthquake include some field observation but are based primarily InSAR imaging and inversion.
Length: Nissen and others (2007) used mapping plus InSAR to estimate a rupture length of 50 km, with models yielding lengths from 45 to 55 km (their table 4). Surface rupture is highly distributed, and likely includes the effects of a triggered *M* 6.7 or subsequent *M* 6+ aftershocks. Splays were noted, but not well mapped and their association with the main shock is not clear. Total system length is ~70 km (Barbot and others, 2008). For table F1, length=50 (45–70) km.

Average displacement from InSAR modeling is 1.8 (1.5-2.2) m. Displacement measurements on western 10 km of InSAR model could include artifacts, which would contribute to the lower *AD* estimate of 1.5 m. Nissen and others (2007) note the problems of tracing fractures and en-echelon tears in forested terrain, so twenty-five percent was added for an upper bound *AD* of 2.2 m.
Depth: InSAR modeling places most of the slip in the upper 9 km. The table F1 depth estimate of 12 km (10–15) includes limitations of the method.
Dip: 71–82 degrees (Barbot and others, 2008, quoting seismic studies) M_w 7.2, right-lateral slip (Barbot and others, 2008).

Pakistan, October 4, 2005

Style: Reverse
Length: 70 km
AD: 5.0 (4.5-5.5) m
Depth: 26 km (from surface)
Dip: 39 (30–45) degrees
Instrumental Magnitude: M_w 7.6
Discussion: Three faults or fault segments combined in low-angle reverse faulting the Balakot-Bagh Fault. Rupture length=70 km from detailed field mapping. *AD* is estimated from an enveloped profile of Kaneda and others (2008). After dip and slope corrections, Kaneda and others (2008) estimate 5.0 m net (dip direction) displacement. Bounds on AD are set at ±10 percent.
Dip: Kaneda and others (2008, p. 541) report dips of 30±10 degrees for near surface features. For instrumental moment estimation, dip=39 degrees on the relevant plane of the moment tensor solution. Dip range: min: 30 degrees, from near-surface estimates, maximum=45 degrees from errors on the CMT. Epicentral depth=26 km from the USGS hypocentral solution. Magnitude M_w 7.6 cited from Kaneda and others (2008).

Wenchuan, China, May 12, 2008

Style: Reverse Oblique
Length: 240 (232–330) km
AD: 3.85 (3.48–4.2) m
Depth: 20 km (vertical)
Dip: 50 (42-60) degrees
Instrumental Magnitude: M_w 7.9
Discussion: Main trace surface rupture of the Longmen Shan system was 240 km long. Rupture was duplexed over 72 km of that distance on the Pengguan Fault. Modeling of InSAR and GPS indicate the coseismic rupture continued northward another 90 km (Qi and others, 2011; Xu and others, 2009). Sense of slip and coseismic rupture extent are from Yu and others (2009). Slip estimates from surface rupture, InSAR, and GPS joint inversion are from Xu and others (2010).
Dip: 42-60 degrees is from InSAR and GPS (Xu and others 2010; Qi and others, 2011). Depth estimate is from Qi and others (2011), who model the base of the reverse fault at 20 (18–24) km; slip may continue eastward on a subhorizontal plane. Qi and others (2011) modeling puts some slip 70-80 km down-dip.
AD on the main trace: 3.48 m minimum from measurements. *AD* on the subparallel Pengguan Fault is 1.09 m, from displacement measurements. The Pengguan rupture could be counted as a main trace extension or as an increase to the *AD* of the main trace. Put end-to-end with the main trace gives 312 km length, *AD* 2.95 m, and a best *AD*=3.3 m that includes 10 percent in enveloping of the main trace measurements. The shortest surface rupture and largest *AD* would add Pengguan to main trace displacements because the sense of the motion is similar, giving 3.84 m *AD* averaged over 240 km. The upper *AD* estimate of 4.2 m is ten percent more, from approximate enveloping of the rupture profile. *AD* over the whole rupture is likely to be smaller if the northern 90 km is included.

El Mayor-Cucapah, Baja California, Mexico, April 4, 2010

Style: SSRO
Length: 117 (115–120) km
AD: 1.88 (1.7–2.1) m
Depth: 10 (9–17) km
Dip: 65 (55–75) degrees
Instrumental Magnitude: M_w 7.17
Discussion: Rupture was right-lateral on the Borrego and Pescadores Faults within the Sierra Cucapah. A linking normal fault joins the two. Dips are in opposite senses, dipping east to the south, and west to the north of the join. M_o: 7.28×10^{19} N*m, M_w 7.17. Length is 117 km based on SAR and SPOT airborne observations. Minimum and maximum lengths (115, 120 km, respectively) are extrapolations of the displacement profile in Wei and others (2011). *AD* from measurements is 1.88 m. With 10 percent increase by enveloping, upper *AD* estimate is 2.1 m. Lower *AD* estimate is -10 percent, or 1.7 m.
Dip: 65 (55–75) degrees. Wei and others (2011) give dips in three sections: 51 km dips 75° E., 60 km dips 60° W., and 18 km dips 50° E.

Depth: Wei and others (2011) report, "Overall, most of the energy release occurred at depths of less than 9 km…." Depth estimate in table F1, 10 (9–17) km is chosen because some energy does radiate from deeper in the models.

Darfield, New Zealand, September 4, 2010

Style: SSR
Length: 29.4 (29.4–31.5) km
AD: 2.5 (2.4–2.7) m
Depth: 15 (12–18) km
Dip: 90 (67–100) degrees
Instrumental Magnitude: M_w 7.1
Discussion:
Length: 29.5 km linear, 31.5 km counting overlaps in the rupture profile.
AD: 2.54 m computed from Quigley and others (2012). The range of 2.4–2.7 m *AD* is from estimates of the effect of the averaging and enveloping methods on computing *AD* from the scattered field points.
Dip: Subvertical SS from seismic indications, but GPS field is fit best by a plane dipping at 67 degrees. Magnitude from van Dissen and others (2011).

Adjustments to Earthquakes in Wesnousky (2008)

Length and (or) average displacement were adjusted for four ruptures in Wesnousky (2008).

Fort Tejon, California, January 9, 1857

Style: SSR
Length: 339 km (330–345). Range in length interpreted from the plot of Zielke and others (2010). Zielke and others (2012) report 350 km, but this estimate is thought to not fully remove the 1812 displacements at southeast end of the 1857 rupture.
AD: 4.45 m. Estimated from our digitizing the displacement profile in Zielke and others (2010). Measurements were considered sufficient such that uncertainties were not assigned.
Discussion: Wesnousky (2008) lists this rupture at 360 km in length. This total almost certainly includes at least 20 km of the 1812 rupture on its south end. Zielke and others (2010) give an updated slip distribution for the 1857 rupture based on abundant lidar measurements of 1857 as the most recent event offset.

Landers, California, June 28, 1992

Style: SSR
Length: 63.2 km
AD: 2.8 m

Discussion: The WGCEP 2008 length of the Landers rupture includes displacements on the Burnt Mountain and Eureka Peak Faults. Hough (1994) shows that displacement on these two faults occurred after the Landers main shock as both triggered slip and coseismic slip from a *M* 5.6 aftershock. Thus for ground motion prediction purposes the net length of the Landers rupture should not include these southern components. The table length of 63.2 km considers the southern end of the Johnson Valley rupture to also be the end of the Landers rupture. The average displacement was recalculated from the reduced rupture length.

Hector Mine, California, October 16, 1999

Style: SSR
Length: 44 km, unchanged
AD: 2.0 m
Discussion: The *AD* estimate for the Hector Mine event in Wesnousky (2008) was disputed at the March 2011 UCERF3 Workshop. The Hector Mine rupture profile exhibits extreme spatial variation that must be related to surficial conditions. To approximate slip at a depth below these effects, the displacement profile was enveloped. Surficial properties can also exaggerate displacements, so the envelope attempted to smooth displacements considering both the number of measurement points and the spatial extent of the high and low values.

Denali, Alaska, November 3, 2002

Style: SSR
Length: 341 km
AD: 4.2 (4.0–4.4) m
Discussion: In Haeussler and others (2004) the full earthquake is 341 km long. The additional 39 km compared to the Wesnousky (2008) length of 302 km is from lidar measurements. Haeussler and others (2004) do not show a rupture profile for the lidar extension, which seems to be why it is not was not included in the Wesnousky (2008) length. Lidar imaging that post-dated Haeussler and others (2004) led to revised mapping near the Denali-Totschunda Fault transition (Schwarz and others, 2012). The previous underestimate at the transition averaged 2 m over 15 km. Including this amount in the average displacement calculation increases *AD* to 4.2 (4.0–4.4) m. Other parameters are unchanged from Wesnousky (2008).

Other San Andreas Fault and Southern California Ruptures from Lidar

The purpose for pursuing additional events from lidar measurements is to try to represent as much as possible about known major surface ruptures on California faults. In particular we may ask whether any evidence suggests that earlier ruptures have been remarkably different from more recent, better documented ruptures. Event displacement profiles were extracted from the southern San Andreas Fault (SAF) lidar data (appendix R, this report). Lines were drawn through clusters of lidar displacement points representing 1857 and earlier events. The displacements under the curves and above any

lower event line were adopted as previous event displacement estimates. Two events on the central SAF are identified in this manner, the historical 1812 rupture and a more northerly event thought to have occurred in the 1700s. It is called 1700 arbitrarily.

The historical 1812 event yielded *AD*=2.31 m, with a length of 230 km. The end points are inferred from Weldon (unpub., 2011). The rupture extent of 1812 to the north could extend 30 km farther based on suggestive evidence in the lidar data. If it did extend farther north, it would do so with ~1 m displacement. As a minimum length, we end the rupture short of the Plunge Creek paleoseismic site in San Bernardino, for a total length of 190 km. At this length the average displacement would be 2.4 m. To the south, Yule and others (2006) suggests 1812 displacements of ~0.5 m at Burro Flats. If so, the southern end of the 1812 rupture must be near; 10 km is allowed beyond the Burro Flats site. This gives an upper length estimate of 270 km—length: 230 (190–270) km.

Uncertainty in *AD* could be half a meter more or less but not a meter for most of the rupture length, allowing different opinions for how to draw the event line through lidar points. Also, the rupture displacements are pinned at Burro Flats, Cajon Pass, and Wrightwood. The net range of average displacements is estimated to be 1.8 to 2.8 m.

The 1700 rupture is estimated to have been 230 (210–280) km long. The maximum length comes from the north end potentially being 20 km longer than the preferred estimate, north of which the San Andreas Fault enters a creeping section of the fault. The southern extent could be up to 30 km longer; were it any more, there would be more evidence for it in the central part of the rupture trace where rupture offsets tend to be well preserved. The total length could be 20 km shorter within lidar uncertainties. *AD* for the respective length estimates is 3.5 (2.5–3.8) m.

A southernmost SAF event is inferred from Mojave and San Bernardino lidar south to Burro Flats, plus limited additional stream offset measurements farther south. From paleoseismic investigations this event is believed to have occurred near A.D. 1690. This event appears to have been 235 (220–250) km long with an average displacement of 4 (3.5–4.5) m.

The most recent large San Jacinto Fault rupture is also evident in the lidar data (appendix R, this report; Salisbury and others, 2012). This event was 80 (76–85) km long with 2 (1.8–2.2) m average displacement.

References Cited in Supplement

Allen, C., Zhuoli, L., Hong, Q., Xueze, W., Huawei, Z., and Weishi, H., 1991, Field study of a highly active fault zone—The Xianshuiehe fault of southwestern China: Geological Society of America Bulletin, v. 103, p. 1178–1198.

Arrowsmith, J.R., Crosby, C.J., Korjenkov, A.M., Mamyrov, E., Povolotskaya, I.E., 2005, Surface rupture of the 1911 Kebin (Chon-Kemin) earthquake, Northern Tien Shan, Kyrgyzstan [abs.]: Eos (American Geophysical Union Transactions), v. 86, no. 52, Fall meeting supplement, abs. T51F-05 [PowerPoint presentation], 19 p., accessed August 25, 2011, at *http://activetectonics.asu.edu/N_tien_shan/05AGU_kyrgyzstan_cjc.ppt*.

Baljinnyam, I., Bayasgalan, A., Borisov, B.A., Cisternas, A., Dem'yanovich, M.G., Ganbaatar, L., Kochetkov, V.M., Kurushin, R.A., Molnar, P., Philip, H., and Vashchilov, Y.Y., 1993, Ruptures of major earthquakes and active deformation in Mongolia and its surroundings: Geological Society of America Memoir 181, 62 p.

Barbot, S., Hamiel, Y., and Fialko, Y., 2008, Space geodetic investigation of the coseismic and postseismic deformation due to the 2003 M_w 7.2 Altai earthquake—Implications for the local lithospheric rheology: Journal of Geophysical Research, v. 113, no. B03403, doi:10.1029/2007JB005063.

Beanland, S., and Clark, M., 1994, The Owens Valley fault zone, eastern California, and surface faulting associated with the 1872 earthquake: U.S. Geological Survey Bulletin 1982, 29 p.

Bucknam, R.C., Plafker, G., and Sharp, R.V., 1978, Fault movement (afterslip) following the Guatemala earthquake of February 4, 1976: Geology, v. 6, p. 170–173; doi:10.1130/0091-7613(1978)6.

Chen, W.P., and Molnar, P., 1977, Seismic moments of major earthquakes and average rate of slip in central Asia: Journal of Geophysical Research, v. 82, p. 2954–2969.

Deng, Q., Chen, S., Song, F.M., Zhu, S., Wang, Y., Zhang, W., Burchfiel, B.C., Molnar, P., Royden, L., And Zhang, P., 1986, Variations in the geometry and amount of slip on the Haiyuan fault zone—China and the surface rupture of the 1920 Haiyuan earthquake: Earthquake Source Mechanics Geophysical Monograph, v. 37, p. 169–182.

Engdahl, E.R., and Villasenor, A., 2002, Global seismicity—1900–1999, *in* Lee, W.H.K., Kanamori, H., Jennings, P.C., and Kisslinger, C., eds., The international handbook of earthquake engineering and seismology: Academic Press, p. 665–690.

Funning, G.J., Parsons, B., and Wright, T.J., 2007, Fault slip in the 1997 Manyi, Tibet earthquake from linear elastic modeling of InSAR displacements: Geophysical Journal International, v. 169, p. 988–1008, doi:10.1111/j.1365-246X.2006.03318.x.

Guo, J., Lin, A., Sun, G., and Zheng, J., 2007, Surface ruptures associated with the 1937 *M* 7.5 Tuosuo Lake and the 1963 *M* 7.0 Alake Lake earthquakes and the paleoseismicity along the Tuosuo Lake segment of the Kunlun fault—northern Tibet: Bulletin of the Seismological Society of America, v. 97, p. 474–496, doi:10.1785/0120050103.

Haeussler, P.J., Schwartz, D.P., Dawson, T.E., Stenner, H.D., Lienkaemper, J.J., Sherrod, B., Cinti, F.R., Montone, P., Craw, P.A., Crone, A.J., and Personius, S.F., 2004, Surface rupture and slip distribution of the Denali and Totchunda faults in the 3 November 2002 M 7.9 earthquake, Alaska: Bulletin of the Seismological Society of America, v. 94, no. 6B, p. S23–S52.

Hanks, T.C., and Bakun, W.H., 2002, A bilinear source-scaling model for *M*-logA observations of continental earthquakes: Bulletin of the Seismological Society of America, v. 92, p. 1841–1846.

Hauksson, E., and Shearer, P., 2005, Southern California hypocenter relocation with waveform cross-correlation, part I—Results using the double-difference method: Bulletin of the Seismological Society of America, v. 95, p. 896–903.

Hough, S.E., 1994, Southern surface rupture associated with the *M* 7.3 1992 Landers, California, earthquake: Bulletin of the Seismological Society of America, v. 84, p. 817–825.

Hough, S.E., and Hutton, K., 2008, Revisiting the 1872 Owens Valley, California, earthquake: Bulletin of the Seismological Society of America, v. 98, p. 931–949, doi:10.1785/0120070186.

Hu, Y., 2002, Earthquake engineering in China: Earthquake Engineering and Engineering Vibration, v. 1, no. 1, p. 1–9.

International Seismological Centre, 2013, International seismological centre bulletin 2001 data: International Seismological Centre Web site, accessed July 22, 2013, at *http://www.isc.ac.uk/iscbulletin/*.

Kaneda, H., Nakata, T., Tsutsumi, H., Kondo, H., Sugito, N., Awata, Y., Akhtar, S.S., Majid, A., Khattak, W., Awan, A.A., Yeats, R.S., Hussain, A., Ashraf, M., Wesnousky, S.G., and Kausar, A.B., 2008, Surface rupture of the 2005 Kashmir, Pakistan, earthquake and its active tectonic implications: Bulletin of the Seismological Society of America, v. 98, p. 521–557, doi:10.1785/0120070073.

Katsumata, K., Kasahara, M., Ichiyanagi, M., Kikuchi, M., Sen, R.S., Kim, C.U., Ivaschenko, A., and Tatevossian, R., 2004, The 27 May 1995 M_s 7.6 northern Sakhalin earthquake—An earthquake on an uncertain plate boundary: Bulletin of the Seismological Society of America, v. 94, p. 117–130.

Klinger, Y., 2010, Relation between continental strike-slip earthquake segmentation and thickness of the crust: Journal of Geophysical Research, v. 115, no. B07306, doi:10.1029/2009JB006550.

Klinger, Y., Etchebes, M., Tapponnier, P., and Narteau, C., 2011, Characteristic slip for five great earthquakes: Nature Geoscience, v. 4, p. 389–392, doi:10:1038/NGE01158.

Kurushin, R.A., Bayasgalan, A., Olziybat, M., Enhtuvshin, B., Molnar, P., Bayarsayhan, C., Hudnut, K., and Lin, J., 1997, The surface rupture of the 1957 Gobi-Altay, Mongolia, earthquake: Geological Society of America Special Paper 320, 143 p.

Lawson, A.C., chairman, 1908, The California Earthquake of April 18, 1906—Report of the State Earthquake Investigation Commission, vol. I and II: Washington, D.C., Carnegie Institution of Washington, 451 p.

Liu-Zeng, J., Klinger, Y., Xu, X., Lasserre, C., Chen, G., Chen, W., Tapponnier, P., and Zhang, B., 2007, Millennial recurrence of large earthquakes on the Haiyuan fault near Songshan, Gansu Province, China: Bulletin of the Seismological Society of America, v. 97, p. 14–34, doi:10.1785/0120050118.

Nissen, E., Emmerson, B., Funing, G.J., Mistrukov, A., Parsons, B., Robinson, D.P., Rogozhin, E., and Wright, T.J., 2007, Combining InSAR and seismology to study the 2003 Siberian Altai earthquakes—Dextral strike-slip and anti-clockwise rotations in the northern India-Eurasia collision zone: Geophysical Journal International, v. 169, p. 216–232.

Papadimitriou, E., Wen, X., Karakostas, V., and Jin, X., 2004, Earthquake triggering along the Xianshuihe fault zone of western Sichuan, China: Pure and Applied Geophysics, v. 161, p. 1683–1707.

Peltzer, G., Crampe, F., and King, G., 1999, Evidence of nonlinear elasticity of the crust from the M_w 7.6 Manyi (Tibet) earthquake: Science, v. 286, p. 272–276.

Plafker, G., 1976, Tectonic aspects of the Guatemala earthquake of 4 February 1976: Science, v. 193, p. 1201–1208.

Qi, W., Zuejun, Q., Qigui, L., Freymueller, J., Shaomin, Y., Caijun, X., Yonglin, Y., Xinzhao, Y., Kai, T., and Gang, C., 2011, Rupture of deep faults in the 2008 Wenchuan earthquake and uplift of the Longmen Shan: Nature Geoscience, v. 4, p. 634–640, doi:10.1038/NGE01210.

Quigley, M., Van Dissen, R., Litchfield, N., Villamor, P., Duffy, B., Barrell, D., Furlong, K., Stahl, T., Bilderback, E., and Noble, D., 2012, Surface rupture during the 2010 M_w

7.1 Darfield (Canterbury) earthquake—Implications for fault rupture dynamics and seismic-hazard analysis, Geology, v. 40, p. 55–58, doi:10:1130/G32528.1.
Richter, C.F., 1958, Elementary seismology: San Francisco, W.H. Freeman, Co., 768 p.
Salisbury, J.B., Rockwell, T.K., Middleton, T.J., and Hudnut, K., 2012, LiDAR and field observations of slip distribution for the most recent surface ruptures along the central San Jacinto fault: Bulletin of the Seismological Society of America, v. 102, p. 598–619, doi:10.1785/0120110068.
Schlupp, A., and Cisternas, A., 2007, Source history of the 1905 great Mongolian earthquakes: Geophysical Journal International, v. 169, p. 1115–1131.
Schwartz, D.P., Haeussler, P.J., Seitz, G.G., and Dawson, T.E., 2012, Why the 2002 Denali fault rupture propagated onto the Totschunda fault—Implications for fault branching and seismic hazards: Journal of Geophysical Research, v. 117, no. B11, 304 p.
Schwartz, D.P., Hecker, S., and Ponti, D., 2009, The July 23, 1905, Bulnay fault, Mongolia surface rupture: Seismological Research Letters, v. 80, p. 357.
Shimamoto, T., Watanabe, M., Suzuki, Y., Kozhurin, A.I., Strel'tsov, M.I., and Rogozhin, E., 1996, Surface faults and damage associated with the 1995 Neftegorsk earthquake: Journal of the Geological Society of Japan, v. 102, no. 10, p. 894–907.
Song, S.G., Beroza, G.C., and Segall, P., 2008, A unified source model for the 1906 San Francisco earthquake: Bulletin of the Seismological Society of America, v. 98, p. 823–831.
Thatcher, W., Marshal, G., and Lisowski, M., 1997, Resolution along the 470-km-long rupture of the great 1906 San Francisco earthquake and its implications: Journal of Geophysical Research, v. 102, p. 5353–5367.
Van Dissen, R., Barrell, D., Litchfield, N., Villamor, P., Quigley, M., King, A., Furlong, K., Begg, J., Townsend, D., Mackenzie, H., Stahl, T., Noble, D., Duffy, B., Bilderback, E., Claridge, J., Klahn, A., Jongens, R., Cox, S., Langridge, R., Ries, W., Dhakal, R., Smith, A., Horblow, S., Nicol, R., Pedley, K., Henham, H., Hunter, R., Zajac, A., Mote, T., 2011, Surface rupture displacement on the Greendale Fault during the M_w 7.1 Darfield (Canterbury) earthquake, New Zealand, and its impact on man-made structures: Auckland, New Zealand: Ninth Pacific Conference on Earthquake Engineering: Building an Earthquake-Resilient Society, April 14–16, 8 p.
Vergnolle, M., Pollitz, F., and Calais, E., 2003, Constraints on the viscosity of the continental crust and mantle from GPS measurements and postseismic deformation models in western Mongolia: Journal of Geophysical Research, v. 108, no. B10, 2502, p. 15-1–15-12, doi:10.1029/2002JB002374.
Vittori, E., Carver, G.A., Jayko, A.S., Michetti, A.M., and Slemmons, D.B., 2003, Quaternary fault map of Owens Valley, eastern California [abs.]: 16th International Union Quaternary Research Conference Programs with Abstracts, p. 106.
Wald, D.J., Kanamori, H., Helmberger, D.V., and Heaton, T.H., 1993, Source study of the 1906 San Francisco earthquake: Bulletin of the Seismological Society of America, v. 83, p. 981–1019.
Wang, H., Xu, C., and Ge, L., 2007, Coseismic deformation and slip distribution of the 1997 M_w 7.5 Manyi, Tibet, earthquake from InSAR measurements: Journal of Geodynamics, v. 44, p. 200–212, doi:10.1016/j.jog.2007.03.003.

Wei, S., Fielding, E., Leprince, S., Sladen, A., Avouac, J-P., Helmberger, D., Hauksson, E., Chu, R., Simons, M., Hudnut, K., Herring, T., and Briggs, R., 2011, Superficial simplicity of the 2010 El Mayor-Cucapah earthquake of Baja California in Mexico: Nature Geoscience, v. 4, p. 615-618, doi:10.1038/DGEO1213.

Wells, D.L., and Coppersmith, K.J., 1994, New empirical relationships among magnitude, rupture length, rupture width, rupture area, and surface displacement: Bulletin of the Seismological Society of America, v. 84, p. 974–1002.

Wen, Y.Y., and Ma, K-F., 2010, Fault geometry and distribution of asperties of the 1997 Manyi, China (M_w=7.5), earthquake—Integrated analysis from seismological and InSAR data: Geophysical Research Letters, v. 37, no. L05303, doi:10.1029/2009GL041976.

Wesnousky, S.G., 2008, Displacement and geometrical characteristics of earthquake surface ruptures—Issues and implications for seismic-hazard analysis and the process of earthquake rupture: Bulletin of the Seismological Society of America, v. 98, p. 1609–1632.

Xu, C., Liu, Y., Wen, Y., and Wang, R., 2010, Coseismic slip distribution of the 2008 M_w 7.9 Wenchuan earthquake from joint inversion of GPS and InSAR data: Bulletin of the Seismological Society of America, v. 100, p. 2736–2749, doi:10.1785/0120090253.

Xu, X., Wen, X., Yu, G., Chen, G., Klinger, Y., Hubbard, J., and Shaw, J., 2009, Coseismic reverse- and oblique-slip surface faulting generated by the 2008 M_w 7.9 Wenchuan earthquake, China, Geology, v. 37, p. 515–518, doi:10.1130/G25462A.1.

Yu, G., Xu, X., Klinger, Y., Diao, G., Chen, G., Feng, X., Li, C., Zhu, A., Yuan, R., Guo, T., Sun, X., Tan, X., and An, Y., 2010, Fault-scarp features and cascading-rupture model for the M_w 7.9 Wenchuan earthquake, eastern Tibetan Plateau, China: Bulletin of the Seismological Society of America, v. 100, p. 2590–2614, doi:10.1785/0120090255.

Yule, D., Maloney, S. and Cummings, L.S, 2006, Using pollen to constrain the age of the youngest rupture of the San Andreas fault at San Gorgonio Pass: Seismological Research Letters, v 77, p. 245.

Zhou, H-L., Allen, C.R., and Kanamori, H., 1983, Rupture complexity of the 1970 Tonghai and 1973 Luhuo earthquakes, China, from P-wave inversion, and relationship to surface faulting: Bulletin of the Seismological Society of America, v. 73, p. 1585–1597.

Zielke, O., Arrowsmith, J.R., Ludwig, L.G., Akciz, S.O., 2010, Slip in the 1857 and earlier large earthquakes along the Carrizo Plain, San Andreas fault: Science, v. 327, p. 1119–1122, doi:10.1126/science.1182781.

Zielke, O., Arrowsmith, J.R., Ludwig, L.G., and Akciz, S.O., 2012, High-resolution topography-derived offsets along the 1857 Fort Tejon earthquake rupture trace, San Andreas fault: Bulletin of the Seismological Society of America, v. 102, p. 1135–1154, doi:10.1785/0120110230.